INL/EXT-17-42435 Rev. 0

June 2017

Calculations of hydrogen diffusivity in Zr-based alloys: Influence of alloying elements and effect of stress

J. Yu
C. Jiang
Y. Zhang

INL/EXT-17-42435 Rev. 0

Calculations of hydrogen diffusivity in Zr-based alloys: Influence of alloying elements and effect of stress

J. Yu
C. Jiang
Y. Zhang

June 2017

Idaho National Laboratory
Fuels Modeling and Simulation Department
Idaho Falls, Idaho 83415

Prepared for the
U.S. Department of Energy
Office of Nuclear Energy
Under U.S. Department of Energy-Idaho Operations Office
Contract DE-AC07-99ID13727

ABSTRACT

This report summarizes the progress on calculating hydrogen diffusivity in Zr-based alloys. The presence of hydrogen (H) can detrimentally affect the mechanical properties of many metals and alloys. To mitigate these detrimental effects requires fundamental understanding of the thermodynamics and kinetics governing H pickup and hydride formation. In this work, we focus on H diffusion in Zr-based alloys by studying the effects of alloying elements and stress, factors that have been shown to strongly affect H pickup and hydride formation in nuclear fuel claddings. A recently developed accelerated kinetic Monte Carlo method is used for the study. It is found that for the alloys considered here, H diffusivity depends weakly on composition, with negligible effect at high temperatures in the range of 600-1200 K. Therefore, the small variation in H diffusivity caused by variations in compositions of these alloys is likely not a major cause of the very different H pickup rates. In contrast, stress strongly affects H diffusivity. This effect needs to be considered for studying hydride formation and delayed hydride cracking. This study is supported by the DOE NEAMS program.

Table of Contents

1. Introduction

Zirconium (Zr) alloys are extensively used as fuel cladding tubes in nuclear reactors owing to their low capture cross section to thermal neutron, good mechanical properties, and good corrosion resistance in various environmental conditions [1-3]. Most of current claddings are made of two Zr-based alloys [Zircaloy-2 (Zr2) and Zircaloy-4 (Zr4)]. Zr4 is mainly used in pressurized water reactors (PWRs) and Zr2 in boiling water reactors (BWRs). Significant effort has led to the development of modern Zr-based alloys with improved corrosion resistance and mechanical properties to meet the demands of higher fuel duty. For example, ZIRLO® and M5™ are more resistant to corrosion and hydrogen (H) pickup compared to Zr2 and Zr4, and they are used to replace Zr4 in PWRs. In addition, some other modern Zr-based alloys such as J-alloys and AXIOM™ have also been shown to not have enhanced corrosion at high burnups [1].

An interesting feature of these Zr-based claddings is that the addition or variation of a very small amount of alloying elements (typically less than 0.5% in concentration or weight) may be sufficient to dramatically change the corrosion behavior and/or H pickup fraction [1, 2] under operating conditions. For instance, with higher Fe content substituted for Ni, Zr4 (Zr-1.5Sn-0.2Fe-0.1Cr in wt%)] was developed with significantly lower H pickup fraction compared to that exhibited by Zr-2 (with an approximate composition of Zr-1.5Sn-0.14Fe-0.10Cr-0.06Ni in wt%). For H to accumulate in the metal matrix of claddings, it needs to be produced during oxidation, and then diffuse over the oxide layer and eventually in the metal matrix. Therefore, the very different H pickup rates in various Zr-based alloys could be caused by 1) different oxidation kinetics and thus H production rates, 2) different transport speeds over the oxide layer [1] though the oxide which by itself is generally an effective barrier to the absorption of hydrogen [3], and 3) different diffusion speeds in the metal matrix. However, it is not clear how the alloying elements will affect H diffusion, which is one of focuses in this study.

Another factor that may strongly affect H diffusion is stress. For instance, during hydride formation, stress may be induced by the mismatch between hydrides and the Zr matrix [3]. Upon cyclic thermal and mechanical loadings, hydrides can dissolve and reorient; this process involves H diffusion with the presence of stress. Meanwhile, stress may also be concentrated at crack tips during delayed-hydride-cracking (DHC). Zr-based alloy cladding tubes used in the nuclear industry are highly susceptible to DHC, which occurs when dissolved H atoms diffuse along the stress gradient towards the tensile stress concentration region at the crack tip, followed by reformation of hydrides at the crack tip and subsequent fracture [3, 4]. DHC may take place at stress levels much lower than the yielding stress and has remained to be a concern for cladding integrity during used fuel storage. A more comprehensive understanding on hydride reorientation and DHC requires a fundamental understanding of the stress state effect on the H diffusion.

In the past, a plethora of investigations on understanding of H diffusion in α-Zr and Zr alloys has been reported in the literature. However, most investigations were relied on experimental measurements [5-9]. It has been commonly accepted that H diffuses in Zr alloys via the same mechanism as in α-Zr, with additional trapping caused by alloying elements and impurities. Due to the hexagonal symmetry of α-Zr, the diffusivity of H along <c> usually differs from that along <a> (in a plane parallel to <a> and normal to <c>), with the former suggested to be higher than the latter with $D_c/D_a>1$ but not exceeding 2 at temperatures above 600 K by Kearns et al. [8]. In addition to these experiments, atomic scale studies such as density functional theory (DFT) calculations have also been applied to H diffusion in α-Zr [10-12].

H diffusion in α-Zr involves multiple hopping paths coupled with each other for long-range diffusion. The hopping rates obtained from DFT calculations need to be incorporated into either analytical theories or other modeling methods such as kinetic Monte Carlo (KMC) to predict diffusivity. One challenge to apply KMC to H diffusion in hcp metals is that the potential energy surface contains an energy basin formed by neighboring tetrahedral sites, which strongly limits the efficiency of KMC at low temperatures due to basin trapping. Since accurate H diffusivity is highly desired at low temperatures [4] to predict the kinetics of DHC, which is active in the temperature range of about 150 to 300 °C, acceleration of KMC is needed. Although guidance for general acceleration approaches already exists in the literature [13], analytical solutions that directly apply to interstitial diffusion in hcp crystals are yet to be derived. Recently an accelerated KMC method was developed for H diffusion in hcp metals by co-authors of this study [14]. Parameterized by DFT calculations, the accelerated KMC method is capable of efficiently calculating H diffusivity in a variety of Zr alloys, without altering the kinetics of long-range diffusion. Using this accelerated KMC method, this report is aimed at modeling H diffusion in Zr-based alloys under the influence of both alloying elements and stress.

2. Methods

The diffusion of H in pure Zr has been discussed in Ref. [14], which is attached as an appendix and contains a detailed introduction about the KMC method used here.

2.1 DFT calculations

To obtain the migration barriers for H diffusion as well as the binding energies between alloying elements (Sn, Fe, Cr, Ni, Nb) and H, we performed *ab initio* calculations using the all-electron projector augmented wave method within the generalized gradient approximation of Perdew, Burke, and Ernzerhof (PBE-GGA) [15], as implemented in VASP [16]. 96-atom supercells, which can be constructed from a 4×4×3 extension of the 2-atom hcp Zr unit cell, are used. Spin-polarized calculations are performed for Fe, Cr and Ni. A plane-wave cut-off energy of 500 eV and a 5×5×5 Monkhorst–Pack *k*-point mesh are used to ensure high numerical accuracy for total energy calculations. All internal atomic positions are fully optimized using a conjugate gradient method until

forces are less than 0.01 eV/Å. Further relaxations of supercell volumes have been found to have negligible effect on the final results. To study the stress effect on H diffusion, the 96-atom hcp Zr supercell is hydrostatically strained by -2%, -1%, 0%, +1% and +2%, respectively. The corresponding hydrostatic stress is 6.2, 2.9, 0, -2.7 and -5.1 GPa, respectively. Such stress levels can be reached at crack tips and at hydride/matrix interfaces. More computational details can be found in Ref. [14].

2.2 Accelerated lattice kinetic Monte Carlo

The accelerated KMC method recently developed by co-authors [14] is used here. For acceleration, the KMC events in basins are replaced using the solutions detailed in Ref. [14]. The calculations are performed from 300 K to 1200 K, one data point every 100 K, covering the temperature range used in previous experiments. To minimize stochastic scattering, at each temperature 100,000 KMC simulations are carried out, each lasting until 100,000 basin exits are detected for sufficient statistics. The averaged mean-square-displacements (MSD) display the expected linear relationship with time, with the slope proportional to diffusivity.

Table 1 Binding energies [eV] between H and vacancy/alloying elements from DFT calculations. Positive (negative) binding energy means attractive (repulsive) interaction. Results for Sn, Fe, Cr, and Ni are from ref. [14].

Element	$E_b^{T_c}$	$E_b^{T_a}$	E_b^{O}
Sn	Not stable [14]	Not stable [14]	-0.037 [14]
Fe	0.094 [14]	0.069 [14]	0.106 [14]
Cr	0.089 [14]	0.065 [14]	0.085 [14]
Ni	0.212 [14]	0.153 [14]	0.165 [14]
Nb	-0.0024	-0.0007	0.042
Vacancy	0.2221	0.2224	0.2807

Table 2 H migration barriers [eV] vs. applied hydrostatic strains and the corresponding stresses [GPa] for 1NN jumps from DFT calculations.

Pressure [GPa]	T-T	T-O	O-T	O-O	Strain %
6.247	0.14592	0.42383	0.45171	0.52806	-2
2.942	0.13576	0.41658	0.3984	0.46177	-1
0	0.12952	0.40612	0.34574	0.39849	0
-2.71	0.1251	0.39299	0.29653	0.33965	+1
-5.134	0.12328	0.37747	0.24796	0.28139	+2

3. Results and discussion

3.1 Results from DFT calculations

The calculated binding energies between H and alloying elements are listed in Table 1. For Sn, Fe, Cr, and Ni, the results have been previously reported in Ref. [14]. As mentioned in Ref. [14], there exist three different interactions between H and an impurity within the first nearest neighbor (1NN) distance. A binding energy of E_b^O represents octahedral (O) H trapped by one impurity site within 1NN distance, $E_b^{T_c}$ is for tetrahedral (T) H interstitials trapped by one impurity site within 1NN distance along <c> and $E_b^{T_a}$ denotes tetrahedral H interstitials trapped by one impurity site within 1NN distance in the basal plane. As shown in Table 1, Fe, Cr and Ni are attractive to H while Sn is repulsive to H. However, the binding energies between H and Nb are unusual. Specifically, the interaction is weakly repulsive when H occupies the tetrahedral sites, but attractive when H is at the octahedral site. As will be shown later by KMC simulations, such unusual feature of the binding energies between H and Nb can lead to lower anisotropic ratio of H diffusivity in Zr alloy system containing Nb element.

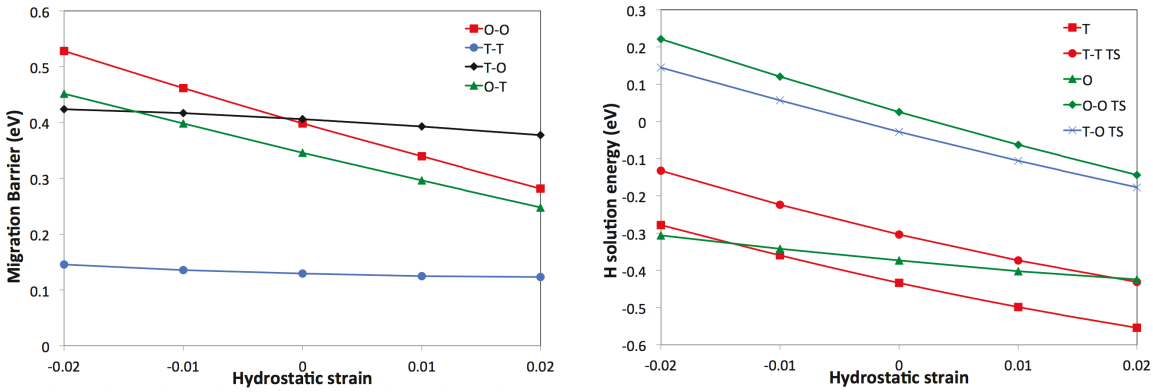

(a) (b)

Figure 1. DFT calculated H migration barrier (a) and H solution energy (b) in hcp Zr as a function of hydrostatic strain.

The activation barriers vs. strain predicted by DFT calculations are given in Table 2 and plotted in Fig. 1(a). Under compressive stress, the activation barriers for all four hopping paths increase. Under tensile stress, the activation barriers for all four hopping paths decrease. It is also shown that, although the activation barriers for all four hopping paths depend nearly linearly on the applied stress, the activation barriers for the O-T and O-O jumps are much more significantly modified by the applied stress compared with T-T and T-O jumps. This can be understood since the O site is significantly larger than the T site and the transition states (TSs) volumetrically. Therefore, the solution energy of a H atom at the O site will exhibit much weaker pressure dependence compared with H at the TS for either O-T or O-O jump (see Fig. 1(b)). Conversely, as shown in Fig. 1(b), H atom at a T site exhibits very similar pressure-dependent behavior as the H atom at the TS for either T-T or T-O jump. The migration barrier, which is the energy difference between

TS and T, therefore shows weak pressure dependence for T-T and T-O jumps. It is also interesting to note that, under compressive stress, the O site can become more favorable than T site for H occupation. This is due to the fact that H energy at T site increases much faster with pressure than at O site.

3.2 Hydrogen diffusion in Zr alloys

KMC simulations are carried out to study the effect of alloy elements on H transport in Zr alloys. The correspondingly approximate concentrations of the alloying elements of Zr alloys used in the KMC simulations are listed in Table 3. J3 (Zr-2.5Nb in wt%) alloy in the family J-Alloys (used extensively in pressure tubes in Canada Deuterium Uranium (CANDU) nuclear reactors [4]) is considered in this study. The results for the three-dimensional H diffusivity and the anisotropic diffusivity ratio in a variety of Zr alloys calculated are plotted in Fig. 2. As shown in Fig. 2 (a), at high temperatures in the range of 600-1200 K, the discrepancy for H diffusivity in all Zr alloys studied here is very small. This indicates that the addition of alloying elements slightly reduces H diffusivity, with negligible effect at high temperatures. This observation is also in line with previous experiments, which found similar H diffusivity in α-Zr, Zr2, and Zr4 [8]. Using $D=D_0\exp(-E_m/K_BT)$ with D_0 being the prefactor and E_m the effective migration barrier, fitting of the KMC results for D_0 and E_m are listed in Table 4. The fitted results agree nicely with previously KMC values of 1.08×10^{-6} m^2/s and 0.46 eV shown in Fig. 2 (a) [14] and the averaged values of 7.0×10^{-7} m^2/s and 0.46 eV for α-Zr and Zircaloy from experiments [8]. At room temperature, the diffusivity of H in Zr2 is significantly lower than in other alloys, presumably due to its higher concentration of Ni that strongly traps H atoms. Intriguingly, the lower H diffusivity in Zr2 than in Zr4 is in contrast with the lower H pickup in the latter. Therefore, the present results suggest that H diffusion in the metal matrix may not be the reason for the very different H pickup in various cladding alloys.

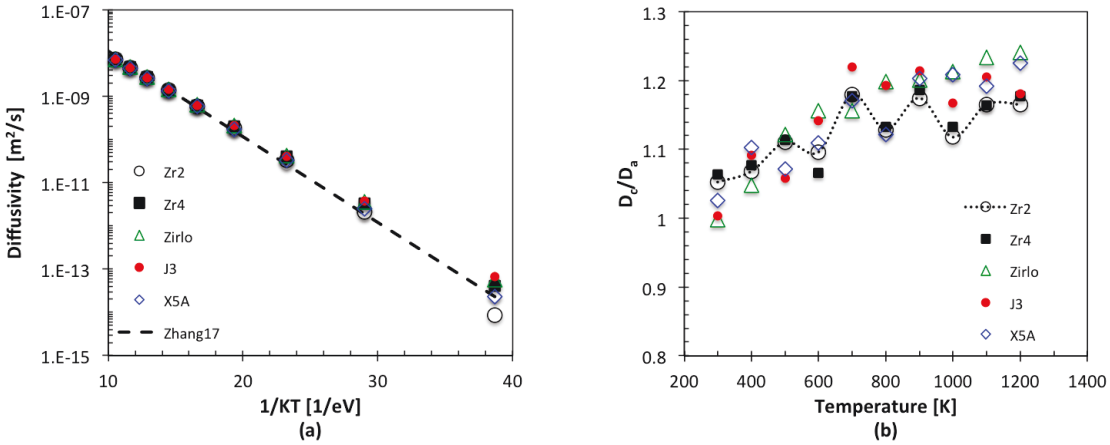

Figure 2. (a) H diffusivity in Zr alloys of Zr2, Zr4, Zirlo, J3 and X5A as a function of inverse temperature, 1/KT; (b) D_c/D_a ratio from 300 to 1200 K.

As shown in Fig. 2 (b), the diffusivity of H is anisotropic, which is in line with previous experiments [8] and KMC results [14]. In particular, the ratio of $D_c/D_a > 1$ is observed at temperatures above 400K. The addition of alloying elements is found to have little effect on the anisotropy. For all alloys studied here, the ratio of D_c/D_a is about 1 at room temperature and increases with increasing temperature. A plateau at about 1.2 is reached at high temperatures, similar to the behavior of H in pure Zr [4]. Some stochastic effect is also noticed in the KMC results shown in Fig. 2(b).

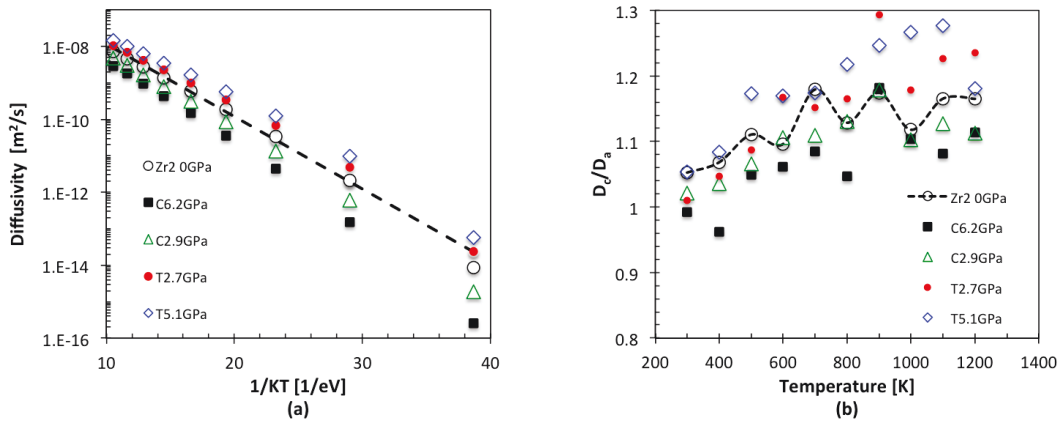

Figure 3. Effect of stress on (a) H diffusivity in Zr2 alloy as a function of inverse temperature, 1/KT; (b) D_c/D_a ratio from 300 to 1200 K.

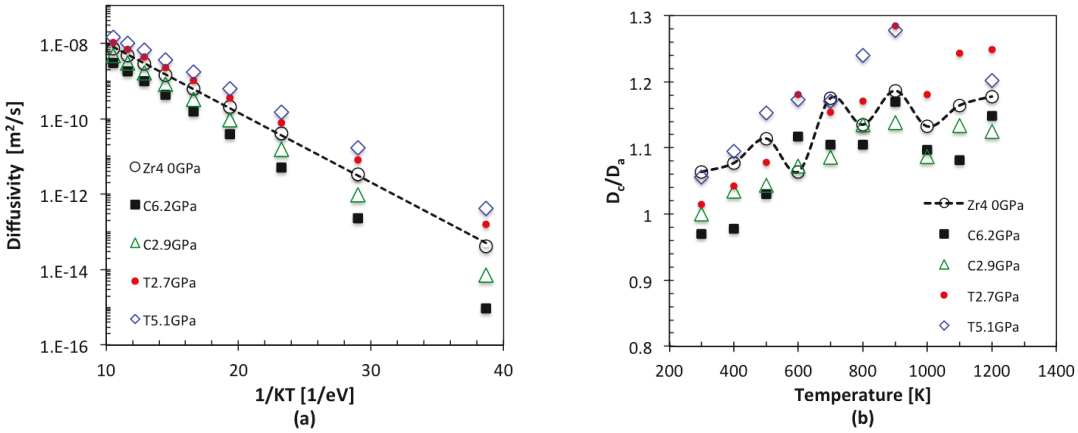

Figure 4. Effect of stress on (a) H diffusivity in Zr4 as a function of inverse temperature, 1/KT; (b) D_c/D_a ratio from 300 to 1200 K.

3.3 Stress effect on hydrogen diffusion

To explore the effect of stress, the diffusivity of H in a variety of Zr alloys with 5 different applied hydrostatic stresses (6.2, 2.9, 0, -2.7 and -5.1 GPa, respectively) have been studied. The KMC simulation results for the stress effect on H diffusivity for Zr2,

Zr4, Zirlo, J3 and X5A alloys are plotted in Figs. 3-7, respectively. As expected, the H diffusivity is reduced under compressive stress and increased under tensile stress. Furthermore, the ratio D_c/D_a depends on both temperature and pressure. In all five Zr alloys considered, a general trend can be seen that both temperature and tensile stress will increase the D_c/D_a ratio and thus promote more anisotropic H diffusion. At room temperature and under compressive stress, the ratio D_c/D_a can also become less than 1.

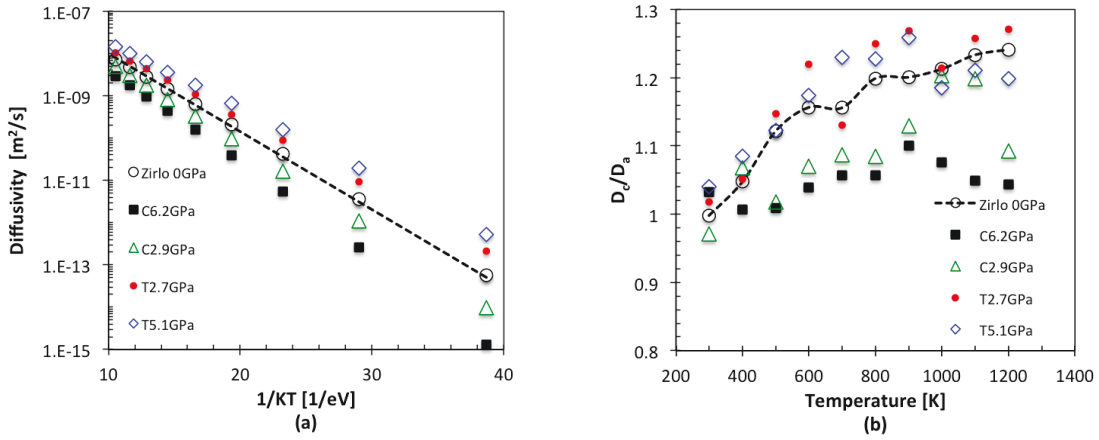

Figure 5. Effect of stress on (a) H diffusivity in Zirlo as a function of inverse temperature 1/KT; (b) D_c/D_a ratio from 300 to 1200 K.

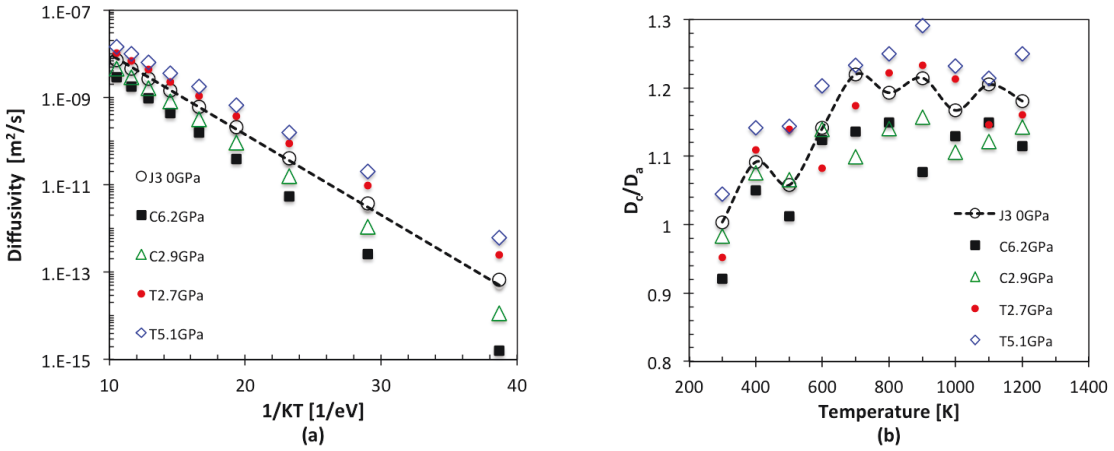

Figure 6. Effect of stress on (a) H diffusivity in J3 as a function of inverse temperature, 1/KT; (b) D_c/D_a ratio from 300 to 1200 K.

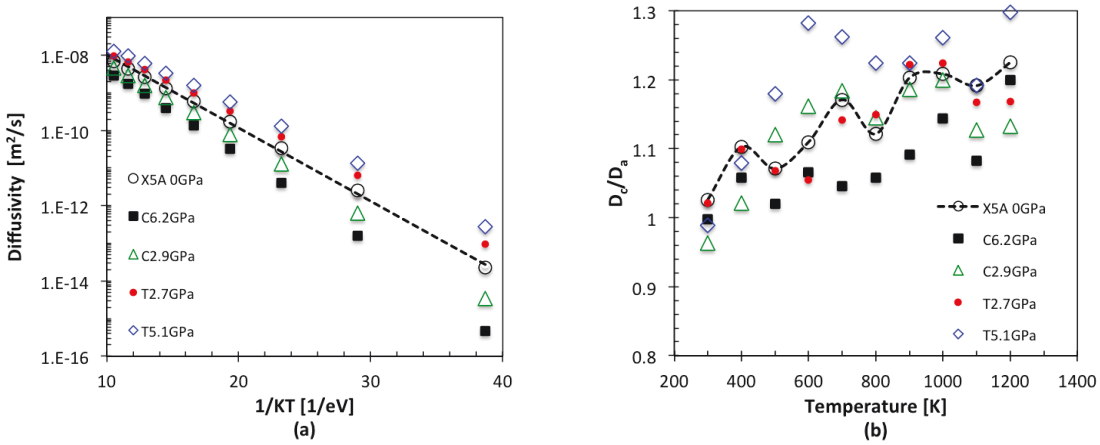

Figure 7. Effect of stress on (a) H diffusivity in X5A as a function of inverse temperature, 1/KT; (b) D_c/D_a ratio from 300 to 1200 K.

3.4 Elastic dipole tensor

It is also desired to have analytical descriptions for the dependence of migration barriers on elastic strain. Based on the theory of linear elasticity, the interaction energy between an external strain field ε_{ij} and a point defect can be calculated from its elastic dipole tensor P_{ij} as [17]:

$$\Delta E = -\sum_{ij} P_{ij}\varepsilon_{ij} \qquad (1)$$

In this study, we have calculated the elastic dipole tensors for H at O, T, and TS positions in hcp Zr using DFT. The results are reported in Table 5 and plotted in Fig. 8. The computational details can be found in Ref. [17]. Due to its low symmetry, the elastic dipole tensor of the TS for the T-O jump is not calculated here. As shown in Fig. 8, results from elastic theory calculations agree quantitatively with direct DFT calculations. Such a good agreement suggests that Eq. (1) can be used to accurately describe H diffusion behavior under an elastic stress field (e.g. around a crack tip) in hcp Zr. It also indicats that the effect of stress on H diffusion is most likely dominated by the elastic interaction.

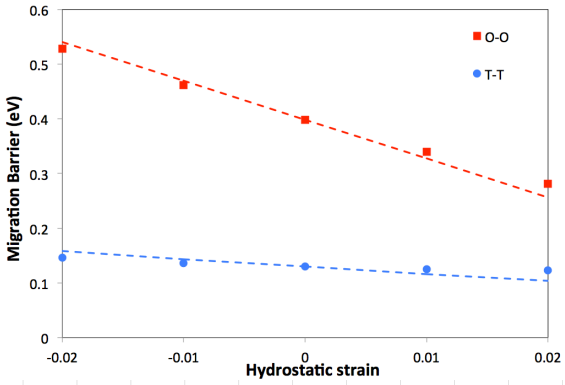

Figure 8. Migration barriers for O-O and T-T paths in hcp Zr as a function of applied hydrostatic strain. Solid symbols are from the present DFT calculations. Solid lines represent results from elastic calculations.

Table 3 Approximate concentrations c_i (atomic fraction) of Sn, Fe, Cr, Ni and Nb in a variety of Zr alloys.

Alloy	Sn	Fe	Cr	Ni	Nb
Zircaloy-2	0.011526	0.002287	0.001754	0.000932	0
Zircaloy-4	0.009990	0.003267	0.001754	0	0
ZIRLO®	0.007684	0.001633	0	0	0.009819
Optimized ZIRLO™	0.005149	0.001633	0	0	0.009819
J-Alloys					
J1	0	0	0	0	0.017674
J2	0	0	0.001754	0	0.015710
J3	0	0	0	0	0.024547
AXIOM™ alloys					
X2	0	0.000980	0	0	0.009819
X5	0.002305	0.005717	0.004386	0.000777	0.006873
X5A	0.003458	0.005717	0.004386	0	0.002946

4. Summary and future work

In this work, an accelerated KMC method is used to reveal the influence of alloying elements and the effect of applied stress on H diffusivity in hcp Zr alloys. It is found that at very low temperature around ambient, H diffusivity depends on the addition of alloying elements. However, at high temperatures in the range of 600-1200 K, the discrepancy for H diffusivity in all of Zr alloys studied here is very small. This indicates that the addition of alloying elements has negligible effect at high temperatures on H

diffusivity, and this is likely not the reason for the very different H pickup in various cladding alloys. Applied stress is found to have a stronger effect on H diffusion than alloying elements. H diffusivity decreases under compressive and increases under tensile stress. Such change in H diffusion needs to be considered at stress fields induced by crack tips or hydrides.

Table 4 Fitting of the KMC results using $D=D_0\exp(-E_m/K_BT)$

	D_0 [m^2/s]	E_m [eV]
Zhang17 [14]	1.08×10^{-6}	0.46
Zr2	1.08×10^{-6}	0.457
Zr4, ZRILO, J3	7.0×10^{-7}	0.425
X5A	9.0×10^{-7}	0.448

Table 5 Elastic dipole tensors P_{ij} for H at various interstitial sites and transition states in hcp Zr.

Site	P_{11} [eV]	P_{22} [eV]	P_{33} [eV]
T	1.999	1.999	3.265
O	0.779	0.779	1.313
T-T TS	3.404	3.404	1.174
O-O TS	3.105	3.105	3.801

In order to develop a more comprehensive understanding on the H diffusion in Zr-based alloys, the thrust areas planned and required further and rigorous investigations are the following:

1) The effect of vacancy on the H diffusion. DFT calculations for binding energies between H and vacancy were finished and results are also listed in Table 1. It is clear that vacancy is attractive to H strongest. Such strong H trapping is expected to impede the H diffusion significantly. Corresponding KMC simulations are being carried out to investigate the influence of vacancy and alloy elements on H transport in Zr alloys.
2) The effect of oxygen on the H diffusion. DFT calculations for binding energies between H and oxygen will be carried out. Corresponding KMC simulations will be carried out to investigate the effect of oxygen and alloy elements on H transport in Zr alloys. In addition, H difusivity in M5 alloy will also be studied.
3) The influence of oxygen, vacancy and alloy elements on H transport in Zr alloys. This aim will be done via carrying out KMC simulations.
4) The influence of applied stress, oxygen, vacancy and alloy elements on H transport in Zr alloys. This thrust will be finished by performing KMC simulations.

We note that a complete framework for hydrogen pick up also requires robust models for oxidation of Zircaloys and H transport through the oxide layers.

5. References

1. Motta, A.T., A. Couet, and R.J. Comstock, *Corrosion of Zirconium Alloys Used for Nuclear Fuel Cladding.* Annual Review of Materials Research, 2015. **45**(1): p. 311-343.
2. Zinkle, S.J., K.A. Terrani, and L.L. Snead, *Motivation for utilizing new high-performance advanced materials in nuclear energy systems.* Current Opinion in Solid State & Materials Science, 2016. **20**(6): p. 401-410.
3. Allen, T., R. Konings, and A. Motta, *Corrosion of Zirconium Alloys.* Comprehensive Nuclear Materials, 2012. **5**: p. 49-68.
4. Chan, K.S., *An assessment of delayed hydride cracking in zirconium alloy cladding tubes under stress transients.* International Materials Reviews, 2013. **58**(6): p. 349-373.
5. Sawatzky, A., *The diffusion and solubility of hydrogen in the alpha-phase of zircaloy-2.* Journal of Nuclear Materials, 1960. **2**(1): p. 62-68.
6. Schwartz, C.M. and M.W. Mallett, *Observations on the behavior of hydrogen in zirconium.* Transactions of the American Society for Metals, 1954. **46**: p. 640-654.
7. Kearns, J.J., *Terminal solubility and partitioning of hydrogen in alpha phase of zirconium zircaloy-2 and zircaloy-4.* Journal of Nuclear Materials, 1967. **22**(3): p. 292-303.
8. Kearns, J.J., *Diffusion coefficient of hydrogen in α-Zr, Zircaloy2 and Zircaloy4.* Journal of Nuclear Materials, 1972. **43**(3): p. 330-338.
9. Zhang, C.S., B. Li, and P.R. Norton, *The study of hydrogen segregation on Zr(0001) and Zr(10(1)over-bar0) surfaces by static secondary ion mass spectroscopy, work function, Auger electron spectroscopy and nuclear reaction analysis.* Journal of Alloys and Compounds, 1995. **231**(1-2): p. 354-363.
10. Sholl, D.S., *Using density functional theory to study hydrogen diffusion in metals: A brief overview.* Journal of Alloys and Compounds, 2007. **446**: p. 462-468.
11. Christensen, M., et al., *H in alpha-Zr and in zirconium hydrides: solubility, effect on dimensional changes, and the role of defects.* Journal of Physics-Condensed Matter, 2015. **27**(2): p. 025402.
12. Domain, C., R. Besson, and A. Legris, *Atomic-scale Ab-initio study of the Zr-H system: I. Bulk properties.* Acta Materialia, 2002. **50**(13): p. 3513-3526.
13. Puchala, B., M.L. Falk, and K. Garikipati, *An energy basin finding algorithm for kinetic Monte Carlo acceleration.* Journal of Chemical Physics, 2010. **132**(13): p. 134104.
14. Zhang, Y.F., C. Jiang, and X.M. Bai, *Anisotropic hydrogen diffusion in alpha-Zr and Zircaloy predicted by accelerated kinetic Monte Carlo simulations.* Scientific Reports, 2017. **7**: p. 41033.
15. Perdew, J.P., K. Burke, and M. Ernzerhof, *Generalized gradient approximation made simple.* Physical Review Letters, 1996. **77**(18): p. 3865-3868.
16. Kresse, G. and J. Furthmuller, *Efficient iterative schemes for ab initio total-energy calculations using a plane-wave basis set.* Physical Review B, 1996. **54**(16): p. 11169-11186.
17. Agarwal, R. and D.R. Trinkle, *Light-element diffusion in Mg using first-principles calculations: Anisotropy and elastodiffusion.* Physical Review B, 2016. **94**(5): p. 054106.

6. Appendix: Anisotropic Hydrogen Diffusion In A-Zr And Zircaloy Predicted By Accelerated Kinetic Monte Carlo Simulations

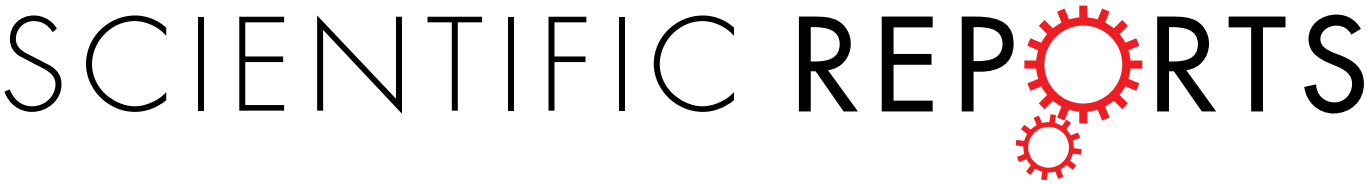

OPEN

Anisotropic hydrogen diffusion in α-Zr and Zircaloy predicted by accelerated kinetic Monte Carlo simulations

Received: 21 October 2016
Accepted: 14 December 2016
Published: 20 January 2017

Yongfeng Zhang[1], Chao Jiang[1] & Xianming Bai[2]

This report presents an accelerated kinetic Monte Carlo (KMC) method to compute the diffusivity of hydrogen in hcp metals and alloys, considering both thermally activated hopping and quantum tunneling. The acceleration is achieved by replacing regular KMC jumps in trapping energy basins formed by neighboring tetrahedral interstitial sites, with analytical solutions for basin exiting time and probability. Parameterized by density functional theory (DFT) calculations, the accelerated KMC method is shown to be capable of efficiently calculating hydrogen diffusivity in α-Zr and Zircaloy, without altering the kinetics of long-range diffusion. Above room temperature, hydrogen diffusion in α-Zr and Zircaloy is dominated by thermal hopping, with negligible contribution from quantum tunneling. The diffusivity predicted by this DFT + KMC approach agrees well with that from previous independent experiments and theories, without using any data fitting. The diffusivity along <c> is found to be slightly higher than that along <a>, with the anisotropy saturated at about 1.20 at high temperatures, resolving contradictory results in previous experiments. Demonstrated using hydrogen diffusion in α-Zr, the same method can be extended for on-lattice diffusion in hcp metals, or systems with similar trapping basins.

The diffusion of hydrogen in hcp metals has attracted extensive research interests for both its scientific merit and technological importance. It is the rate-limiting step for solid hydrogen storage in Mg based alloys[1] and for mechanical property degradation in Ti[2] and Zr alloys[3]. For instance, Zr-based alloys such as Zircaloy2 and Zircaloy4 (denoted as Zircaloy) are widely used as the cladding of fuel rods in nuclear reactors for their excellent corrosion resistance and very low absorption cross-section of thermal neutrons. During their service time, these alloys operate in extremely harsh environments, combining high temperatures and corrosive coolants such as water. In light water reactors, Zircaloy claddings directly contact coolant water, with a local temperature at the interface of about 400 °C. Consequently, Zircaloy react with water, producing an oxide layer at the interface and hydrogen (H), of which a substantial fraction infiltrates into the cladding interior[3]. Due to the low solubility of H in α-Zr, which is the main component of claddings, hydrides precipitate in the cladding matrix[4–6]. Hydride formation can detrimentally affect the cladding integrity primarily in two ways. First, the formation of hydrides reduces the fracture toughness of the cladding matrix[7,8], increasing the probability of fuel failure when fuel-cladding mechanical interaction (PCMI) occurs during fuel operation. Second, upon cyclic thermal and mechanical loadings, hydrides can dissolve and reorient. During used-fuel storage, fracture may propagate via the so-called delayed-hydride-cracking (DHC) mechanism, which is induced by the dissolving of matrix hydrides and their subsequent re-formation at crack tips[3,9]. To mitigate these detrimental effects requires fundamental understanding of the thermodynamics and kinetics governing hydrogen uptake and hydride formation. In this work, we focus on H diffusion, which is the rate-limiting factor for both hydrogen uptake and DHC.

In the past, understanding of hydrogen diffusion in α-Zr and Zircaloy has relied mostly on experimental measurements[10–15]. It has been commonly accepted that H diffuses in Zircaloy via the same mechanism as in α-Zr, with additional trapping caused by alloying elements and impurities. Due to the differences in the measuring methods and the preparation of samples, scattered data for H diffusivity[10–14] and contradictory results

[1]Fuels Modeling and Simulations, Idaho National Laboratory, Idaho Falls, ID, 83415, USA. [2]Materials Science and Engineering, Virginia Tech, Blacksburg, VA, 24061, USA. Correspondence and requests for materials should be addressed to Y.Z. (email: yongfeng.zhang@inl.gov)

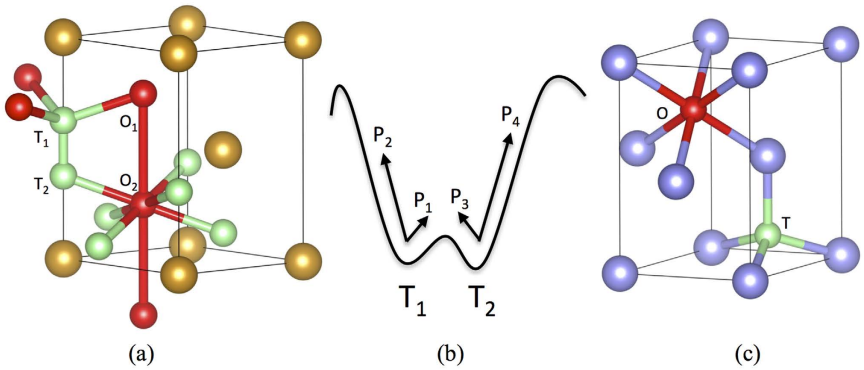

Figure 1. (**a**) The hcp unit cell of Zr (gold) with tetrahedral (green) and octahedral (red) interstitial sites for hydrogen. (**b**) Schematic of an energy basin with two transition states (T_1 and T_2). p_1 (p_3) represents the probability for the system to transition from T_1 to T_2 (T_2 to T_1) in next event. p_2 (p_4) is the probability for the system to exit the basin from the *left* (*right*) side in next event. By definition $p_1+p_2=p_3+p_4=1$. (**c**) 1NN interaction between possible impurity trapping sites (blue) with hydrogen interstitials at tetrahedral and octahedral sites.

regarding the diffusion anisotropy have been reported. Due to the hexagonal symmetry of α-Zr, the diffusivity of H along <c> usually differs from that along <a> (in a plane parallel to <a> and normal to <c>), with the former suggested to be higher than the latter by Kearns *et al.*[14]. However, in a more recent experiment, the latter was reported to be over an order higher than the former[15]. In addition to these experiments, atomic scale studies such as density functional theory (DFT) calculations have also been applied to H diffusion in α-Zr[16–18]. At high temperatures, H diffuses in metals via thermally activated hopping with the hopping rates described by the transition-state-theory (TST). At low temperatures, due to the small mass of H, the contribution from quantum tunneling may become significant[16,19]. The transition temperature is not clear for H in α-Zr. The contribution of thermal hopping at high temperatures can be estimated provided the hopping rates for all involved hopping paths are known. To fully assess the effect of quantum tunneling requires information on the potential energy surface (PES) of H interstitials at energy minima and transition states (TSs) for each hopping path. An alternative approach is to use the semiclassically corrected harmonic-transition-state-theory (SC-HTST) which assumes that the PES is harmonic and requires only the potential energies and vibration frequencies at energy minima and TSs, instead of the full PES[20,21]. The effect of tunneling is accounted for by a correction to the classical thermal hopping rates. For H in α-Zr, the information needed for the SC-HTST approach is not yet available.

H diffusion in α-Zr involves multiple hopping paths coupled with each other for long-range diffusion. The hopping rates obtained from DFT calculations need to be incorporated into either analytical theories or other modeling methods such as kinetic Monte Carlo (KMC) to predict diffusivity. In the literature, several theories have been proposed for H diffusion in hcp crystals[22,23]. These theories give different predictions for H diffusivity. Therefore, they need to be testified to resolve the discrepancies. In this work, we use lattice KMC parameterized by DFT calculations to compute H diffusivity in α-Zr. The KMC method is well known to be capable of providing atomic scale insights on kinetic processes in crystalline solids[24]. In particular, for diffusion on a pre-defined lattice with known hopping rates, KMC is capable of predicting the diffusivity in cases involving multiple jumps and random trapping sites[25,26]. One challenge to apply KMC to H diffusion in hcp metals is that the PES usually contains an energy basin formed by neighboring tetrahedral sites, which strongly limits the efficiency of KMC at low temperatures due to basin trapping. Since accurate H diffusivity is highly desired at low temperatures to predict the kinetics of DHC, which is active in the temperature range of about 150 to 300 °C[27], acceleration of KMC is needed. Although guidance for general acceleration approaches already exists in the literature[28], analytical solutions that directly apply to interstitial diffusion in hcp crystals are yet to be derived.

The objectives of this paper are threefold: (i) to develop an accelerated KMC method for H diffusion in hcp metals, (ii) to obtain H diffusivity in Zr and Zircaloy in a wide range of temperatures, and (iii) to resolve the controversy in previous experiments on H diffusion anisotropy in α-Zr. A systematic understanding of H diffusion in α-Zr is expected by accomplishing these objectives. Although in this work the method is demonstrated using Zr and Zircaloy, the same method can be directly applied to other hcp metals and alloys such as Mg and Ti, provided that the required information for hopping rates are available.

Results

The details of DFT calculations and KMC simulations are provided in the Methods Section. In this section the results are presented.

Hopping rates and impurity trapping from DFT calculations. For α-Zr, the lattice constants are calculated as $c=5.18$ Å and $a=3.24$ Å, agreeing well with previous DFT calculations[17,18,29,30] and experiments[31,32]. Due to its small size, H stays in hcp metals as an interstitial occupying either the tetrahedral (T) site or the octahedral (O) site, as shown in Fig. 1(a). At finite temperatures, both sites are occupied with the partition at thermal equilibrium dictated by the solution energies, and they both are involved in long-range diffusion. Four

Path	E_m (eV)	$\nu_{i,1}$ (THz)	$\nu_{i,2}$ (THz)	$\nu_{i,3}$ (THz)	$\nu_{ts,1}$ (THz)	$\nu_{ts,1}$ (THz)	$\nu_{\pm}$ (THz)
TT	0.129 (0.12[17], 0.129[18])	36.87	36.87	33.06	43.06	43.04	−17.92
TO	0.406 (0.41[17], 0.412[18])	36.87	36.87	33.06	45.80	42.66	−17.59
OT	0.346 (0.35[17])	23.32	20.84	20.84	45.80	42.66	−17.59
OO	0.398 (0.41[17], 0.427[18])	23.32	20.84	20.84	47.30	47.29	−9.95

Table 1. Activation barriers and vibrational frequencies for 1NN jumps from DFT calculations. The activation barriers from refs 17 and 18 are listed in parentheses.

Element	Concentration, c_i	$E_b^{T_c}$	$E_b^{T_a}$	E_b^O
Sn	0.0111	Not stable	Not stable	−0.037 (−0.031[18])
Fe	0.00268	0.094 (0.58[18])	0.069	0.106
Cr	0.00173	0.089 (0.269[18])	0.065	0.085
Ni	0.0003622	0.212 (0.187[18])	0.153	0.165

Table 2. Concentrations (atomic fraction) of Zn, Fe, Cr, and Ni in Zircaloy and their binding energies (eV) with hydrogen. Positive (negative) binding energy means attractive (repulsive) interaction.

hopping paths, namely first nearest neighbor (1NN) TT, TO, OT and OO jumps, are found responsible for the three-dimensional diffusion of H. The activation barriers and vibrational frequencies needed to calculate the hopping rates are predicted by DFT calculations, as listed in Table 1. The activation barriers calculated here agree well with those computed by Domain *et al.*[17] and Christensen *et al.*[18]. In addition to these 1NN jumps, second nearest neighbor (2NN) TT and OO jumps (denoted as TT2 and OO2, respectively) were also suggested in Domain *et al.*[17]. These 2NN jumps are however found to be unstable in this work. Our calculations show that TT2 and OO2 paths spontaneously relax into TO + OT and OT + TO, respectively. Therefore, in our KMC simulations, only 1NN TT, TO, OT and OO jumps are considered. The TT jump has a much lower barrier than others, forming a trapping energy basin in the PES (Fig. 1(b)), which significantly reduces the efficiency of KMC modeling.

Although the absolute solution energy is not needed in KMC simulations, it is calculated in this work for comparisons with the literature. Using Eq. (21) in the Method Section, H solution energy is given as −0.429 eV and −0.366 eV at the tetrahedral and the octahedral site, respectively. Therefore, the tetrahedral site is more stable than the octahedral site for H, with an energetic preference of −0.063 eV, which compares well with the −0.059 eV reported in Domain *et al.*[17] and −0.086 eV in Burr *et al.*[29]. For a more general comparison, most previous DFT calculations[17,18,29,30,33] have predicted that H prefers the tetrahedral site over the octahedral site based on the solution energy as defined in Eq. (21), which was reported to be −0.60 eV in Domain *et al.*[17] and Lumley *et al.*[33], −0.46 eV in Burr *et al.*[29], and −0.52 eV in Udagawa *et al.*[30]. Experimentally, a value of −0.66 eV was suggested[32].

It has been pointed out that while evaluating the relative stability of various H interstitial configurations, the contribution of zero-point-energy (ZPE) in the solution energy should be included due to the small mass of H[18]. At 0 K, the ZPE of a H atom at interstitial site i is given by $\sum_j h\nu_{i,j}/2$. Here h is Planck's constant, and $\nu_{i,j}$ the j_{th} vibration frequency at site i. The summation runs over all three vibrational frequencies at energy minima and only the two real frequencies at TSs. Using the results listed in Table 1, the ZPE within the harmonic approximation is found to be 0.134 eV for the octahedral site, and 0.221 eV for the tetrahedral site, respectively. For the ZPE of H at the O site, our result agrees well with the value (0.123 eV) predicted by Christensen *et al.*[18]. With ZPE included, the octahedral site becomes more stable than the tetrahedral site with an energetic preference of 0.026 eV at 0 K. Such a small difference is actually within the uncertainty caused by the harmonic assumption in DFT calculations. It has been shown by Christensen[18] that by fully taking into account the anharmonic effect, the ZPE at the T site could be reduced from 0.18 eV to 0.166 eV if the neighboring Zr atoms were allowed to relax. A detailed consideration of this anharmonic effect is beyond the scope of this work. Nevertheless, the results indicate that T and O sites are both occupied by H atoms at finite temperatures due to their similar energetic levels.

The binding energies between H and alloying elements such as Sn, Fe, Cr, and Ni are calculated using Eq. (23). The results are listed in Table 2. The concentrations of the alloying elements used in the KMC simulations are also listed. Here, only the 1NN interactions are considered. The 2NN interactions are found to be much weaker than 1NN ones and are therefore neglected. For each type of impurity, three types of 1NN interactions with H exist, depending on the site of H and the relative positions of impurity atoms in reference to the H atom. As shown in Fig. 1(c), H at an octahedral site can be trapped symmetrically by six impurity sites within 1NN distance (number of trapping sites $N_t = 6$) with a binding energy of E_b^O. Tetrahedral H interstitials can be trapped by one impurity site along <c> ($N_t = 1$) with a binding energy of $E_b^{T_c}$, and three others symmetrically ($N_t = 3$) with $E_b^{T_a}$. As shown in Table 2, Fe, Cr and Ni are attractive to H. The presence of these alloying elements will increase the overall H solubility and reduce H diffusivity by trapping H atoms locally. Sn is repulsive to H. In particular, H at the tetrahedral sites surrounding a Sn atom is not stable and automatically relaxes into a nearby interstitial site, meaning that these sites are blocked for H diffusion. Accordingly, the rate for H to jump to these sites is set to be zero in KMC simulations. Except for Ni, the trapping energies calculated here are much lower than those given in Christensen *et al.*[18], which are also listed in Table 2. The comparison is made by comparing with the highest

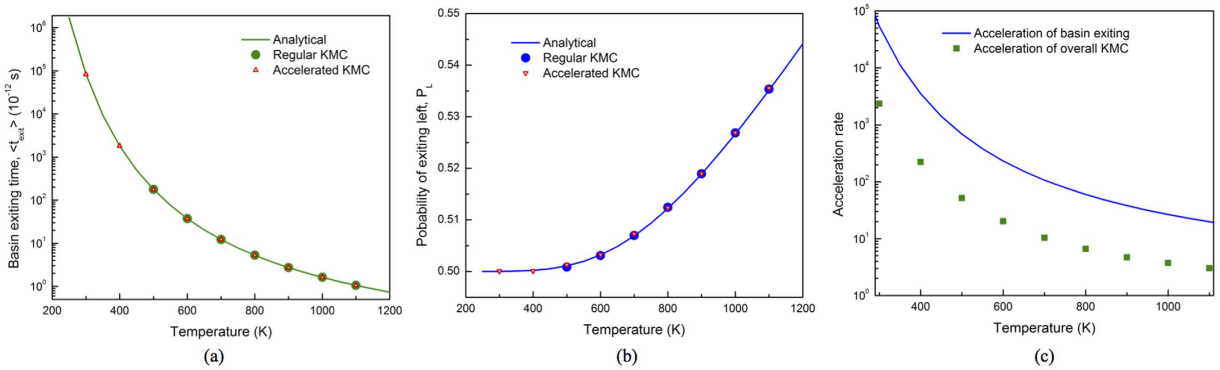

Figure 2. (**a**) Basin exiting time, (**b**) probability of exiting left, and (**c**) acceleration rate as functions of temperature.

binding energies from our calculations for each type of impurity. As will be shown later by KMC simulations, the large trapping energies given by Christensen *et al.* can lead to much lower H diffusivity in Zircaloy than that reported by experiments.

Accuracy and efficiency of accelerated KMC. The key of our accelerated KMC is to replace the time-consuming T-T jumps spent at the energy basins in KMC with the analytical solutions for basin exiting time and probability, as described in the Method Section. Before presenting the results on H diffusivity, the accuracy and efficiency of the accelerated KMC method are demonstrated. To preserve the diffusion kinetics, it is important to reproduce both the average basin exiting time and the exiting probability for each path. Since the analytical solutions in Eqs (16) and (17) are exact, the acceleration is expected to result in no change in the H diffusion kinetics. To confirm this, KMC simulations are carried out every 100 K from 300 K to 1100 K. In each simulation, 100,000 basin exiting events are used to obtain good statistics. As shown in Fig. 2(a,b), for both exiting time and probability, the results from accelerated KMC perfectly match the analytical solutions and the results from regular KMC as well, indicating the correctness of the analytical solutions and the preservation of diffusion kinetics with acceleration. At 300 K and 400 K, regular KMC is too inefficient to get sufficient sampling of KMC events. Still, the results from accelerated KMC follow the analytical solutions.

It is also interesting to note that at low temperature, the hopping rate $\omega_1 \gg \omega_2$ (thus $p_1 \gg p_2$), so that $P_L \cong P_R$ as given by Eq. (17). This implies that after a long trapping time in a basin, the memory of the basin-entering site is lost, leading to nearly equal exiting probability to the *left* (from the path H enters basin) and *right* existing path. However, at high temperatures, the trapping time is short and the escaping probability is biased favoring the basin-entering site. Capturing the escaping probabilities is critical for accurate H diffusivity in hcp crystals. Since exiting to the *left* results in zero net displacement along <c>, overestimate (underestimate) of its probability effectively suppresses (accelerates) H diffusion along <c>, leading to error in both overall diffusivity and diffusion anisotropy.

The average basin exiting time depends on temperature, as does the rate of acceleration relative to regular KMC. At low temperatures, p_1 approaches unity and the acceleration rate n_{acc}, as defined in Eq. (19) in the Method Section, approaches $1/p_2$. It should be noted that the acceleration in Eq. (19) applies only to basin exiting. The computing time for jumps outside the basin remains constant. Therefore, the overall acceleration depends on how often the system visits basins and how long it takes to exit a basin by average. For H in α-Zr, the tetrahedral site is frequently visited since its population is twice of that of the octahedral site, with similar energies for both sites. As shown in Fig. 2(c), the acceleration is significant at low temperatures and decreases upon increasing temperature, mainly because of decreasing basin exiting time as given in Eq. (16). At room temperature, over 2,000 times overall acceleration can be obtained. Even at high temperature such as 800 K, the KMC simulations can still be accelerated by a rate of about 10. Since DHC is usually active in the temperature range of about 150 to 300 °C in Zircaloy claddings[27], acceleration is important for efficient calculations of H diffusivity at low temperatures.

Hydrogen diffusion in pure Zr. The three-dimensional H diffusivity in α-Zr calculated by accelerated KMC is plotted in Fig. 3. The calculations are performed from 300 K to 1100 K, one data point every 100 K, covering the temperature range used in previous experiments. To minimize stochastic scattering, at each temperature 100,000 KMC simulations are carried out, each lasting until 100,000 basin exits are detected for sufficient statistics. The averaged mean-square-displacements (MSD) display the expected linear relationship with time (Fig. 3(a)), with the slope proportional to diffusivity. At high temperatures (>600 K), the KMC results are at the upper bound of the scatter in the experimental data, within a factor of 2 different from most experimental results[10–14], as shown in Fig. 3(b). It should be emphasized that the modeling prediction is based on first principles and is completely independent of the experiments (i.e., no data fitting is used). Thus, this work demonstrates the predictive power of computer modeling. The minor discrepancy between KMC and experiments may come from uncertainty in DFT calculations due to underbinding of GGA or that in experiments due to the differences in measuring method and sample preparation. In particular, in Kearns *et al.* polycrystalline samples with various types of impurities were used[14,34]. Depending on their interactions with H, impurities and grain boundaries may

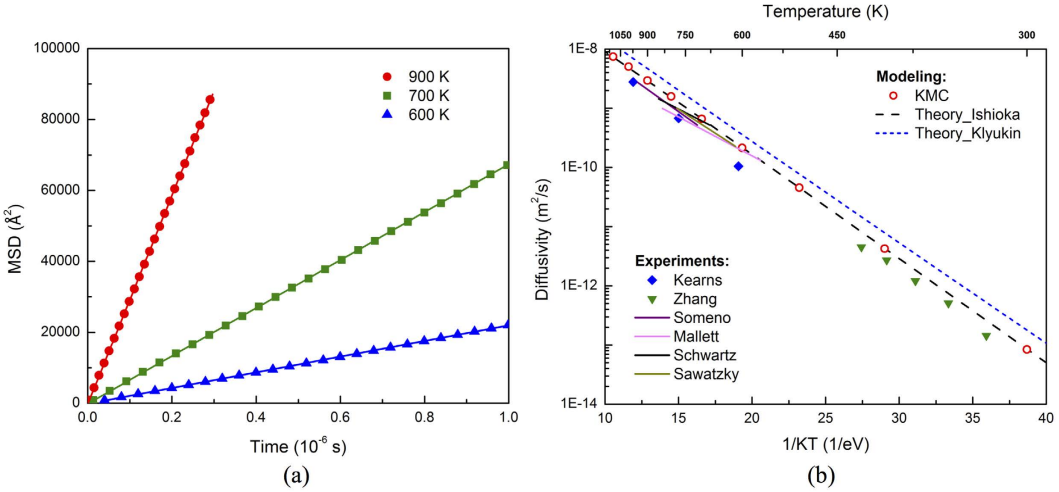

Figure 3. (**a**) Mean-square-displacements (MSDs) of H at 600, 700 and 900 K as functions of time. The symbols are from KMC and lines from linear fitting. (**b**) H diffusivity in α-Zr as a function of inverse temperature, 1/KT.

either facilitate or impede H diffusion. Involving multiple jumps, the diffusivity of H may not necessarily follow the Arrhenius equation. Nevertheless, it is still fitted using the equation $D = D_0 \exp(-E_m/K_BT)$ for comparison with experiments, with D_0 being the prefactor and E_m the effective migration barrier. The fitting of KMC results gives 5.55×10^{-7} m^2/s and 0.41 eV for D_0 and E_m, respectively, agreeing well with the experimental values of $6.94–7.82 \times 10^{-7}$ m^2/s and 0.46–0.47 eV for α-Zr[14]. As will be shown later, better agreement can be achieved by including impurity effects. At low temperatures (<500 K), good agreement between KMC results and experiments[15] is also observed, with the former being higher but no more than a factor of 2 than the latter. It needs to be pointed out that in ref. 15, H diffusivity was measured separately along <a> and <c>, and the overall diffusivity plotted in Fig. 3(b) is converted using Eq. (13). As will be elaborated later, the results on D_c reported by that work was unreasonably low compared to D_a, possibly leading to a low overall diffusivity as well.

Interstitial diffusion in hcp metals involving octahedral and tetrahedral sites has been treated theoretically by different groups. Using an on-lattice random walk model, Ishioka and Koiwa[22] proposed an algorithm to derive the diffusivities of impurity atoms on a crystal lattice containing multiple sublattices, such as the octahedral and tetrahedral sites in hcp crystals. For H in hcp metals, the diffusivities along <c> and <a> directions are given by:

$$\begin{aligned} D_c &= \frac{\omega_{TO}(3\omega_{OO}\omega_{TO} + 2\omega_{OO}\omega_{TT} + 3\omega_{TT}\omega_{OT})}{4(2\omega_{TT} + 3\omega_{TO})(\omega_{TO} + 2\omega_{OT})}c^2 \\ D_a &= \frac{\omega_{TO}\omega_{OT}}{\omega_{TO} + 2\omega_{OT}}a^2 \end{aligned} \quad (1)$$

where the hopping rate ω_{ij} can be calculated using Eq. (5). More recently, starting from Fick's law and considering the balanced flux between equilibrated tetrahedral and octahedral sites, in Klyukin *et al.* an expression was derived for H diffusivity in hcp metal as[23]:

$$D = \frac{1}{2}a^2\omega_{TO}\left(1 + \frac{1}{2}\exp\left(-\frac{\Delta E_{TO}}{K_BT}\right)\right)^{-1} \quad (2)$$

Here ΔE_{TO} is the difference between the solution energies at the tetrahedral and the octahedral sites, including ZPE. K_B is the Boltzmann constant. Note that in Eq. (2) there is no differentiation of D_c and D_a. The parameters listed in Table 1 are used while applying the above theories. As shown in Fig. 3(b), our KMC results agree perfectly with the Ishioka model, which involves all relevant jumps. The Klyukin model is found to overestimate H diffusivity. It ignores the TT and OO jumps and essentially considers only H diffusion along <a>. The overestimation probably comes from the fact that it ignores the time spent for TT and OO jumps.

The above results are obtained without considering quantum tunneling[19,20], which could be important at low temperatures. Given the relatively high barriers for OO and OT jumps, for H diffusion in α-Zr, tunneling is expected to be less important than in some other metals[16]. According to the SC-HTST theory, the contribution of tunneling becomes significant below a critical temperature, $T_c = (h\nu_\pm E_{ZP}/K_B)/(2\pi E_{ZP} - h\nu_\pm \ln 2)$. Here $\nu_\pm$ is the imaginary vibrational frequency at the TS (Table 1), and E_{ZP} the migration barrier with ZPE correction. For TT, TO, OT and OO jumps, the critical temperature is estimated as 72 K, 68 K, 68 K and 38 K, respectively, indicating that tunneling is not significant above room temperature. To better estimate the tunneling effect, Eqs (8) to (10) are applied to the Ishioka theory and in KMC from 300 K to 1100 K. The ratio of tunneling corrected diffusivity (D_T) over that without correction (D) is plotted in Fig. 4. Since the correction factor in Eq. (9) is always larger than 1, so is the ratio of D_T/D. Also, D_T/D decreases with increasing temperature, upon which the tunneling effect diminishes. Above room temperature, the tunneling correction increases H diffusivity by less than 10%, with a

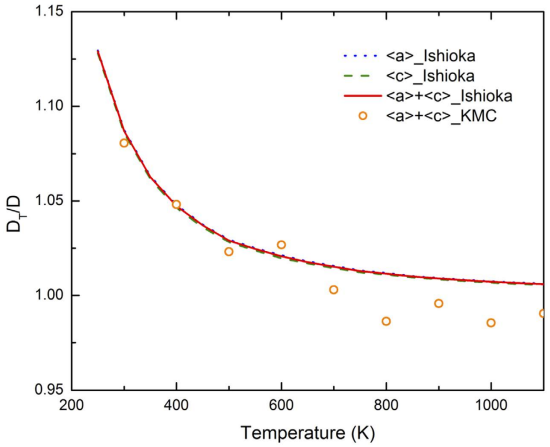

Figure 4. Ratio of tunneling corrected diffusivity (D_T) over that without correction (D).

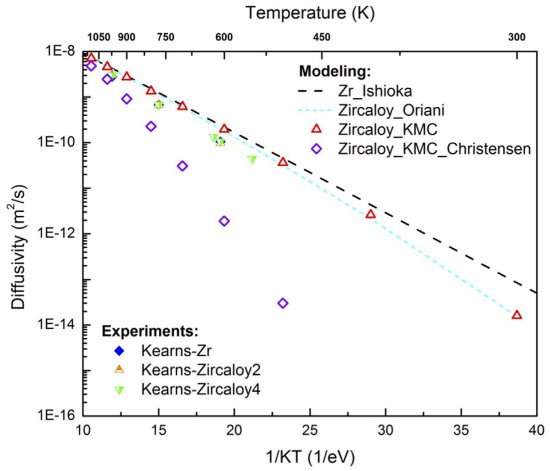

Figure 5. H diffusivity in Zircaloy as a function of inverse temperature, 1/KT.

similar effect along <c> and <a> and thus negligible change in the anisotropy, as shown in Fig. 4. This indicates that above room temperature, H diffusion in α-Zr is dominated by thermally activated hopping. For this reason, H diffusivity will be calculated without considering the tunneling correction in the rest of the paper.

Hydrogen diffusion in Zircaloy. The diffusivity of H in Zircaloy is plotted in Fig. 5. To better compare with the previous experiments, here the concentrations of Sn, Fe, Cr, and Ni are taken as the average values for Zircaloy2 and Zircaloy4 in Kearns *et al.*[34], where the exact compositions of the pure-Zr, Zircaloy2 and Zircaloy4 samples were given. The concentrations used in our KMC calculations are listed in Table 2 in unit of atomic percent. As shown in Fig. 5, with all four alloying elements present, the overall hydrogen diffusivity is reduced, with greater reduction at lower temperatures. Fitting of the KMC results using $D = D_0 \exp(-E_m/K_B T)$ gives 1.08×10^{-6} m^2/s and 0.46 eV for D_0 and E_m, agreeing nicely with the averaged values of 7.0×10^{-7} m^2/s and 0.46 eV for α-Zr and Zircaloy from experiments[14]. The higher fitted migration barrier for Zircaloy in reference to that of pure Zr (0.41 eV) is mainly due to the reduction in diffusivity at low temperatures. In the high temperature region (≥600 K), the reduction as shown by the KMC results is less than 15% (mostly within 10%). Such a small reduction is within the experimental scatter, in good agreement with Kearns *et al.* that H diffusivities in Zr, Zircaloy2 and Zircaloy4 are hardly distinguishable from each other[14]. In the previous experiments, the pure Zr samples contained impurities with very dilute concentrations[34], which may have brought the H diffusion lower and closer to that in Zircaloy. Again, the minor discrepancy between KMC and experiments for Zircaloy could be caused by errors in DFT calculations, or possible presence of other impurities and grain boundaries in experiments.

As shown in Table 2, the binding energies calculated here are quite different from that given in Christensen *et al.*[18]. For a comparison, KMC simulations were also performed with the binding energies taken from ref. 18. As no information about the trapping site was given in ref. 18, in KMC only the trapping of a H atom at a tetrahedral site by a nearby solute atom along <c> direction (with $N_t = 1$) is considered, so that the least trapping (i.e., minimum reduction of H diffusivity) is expected. Still, significant reduction in H diffusivity is observed using the binding energies in ref. 18 (Fig. 5), in contrast to previous experiments that showed similar H diffusivity in α-Zr

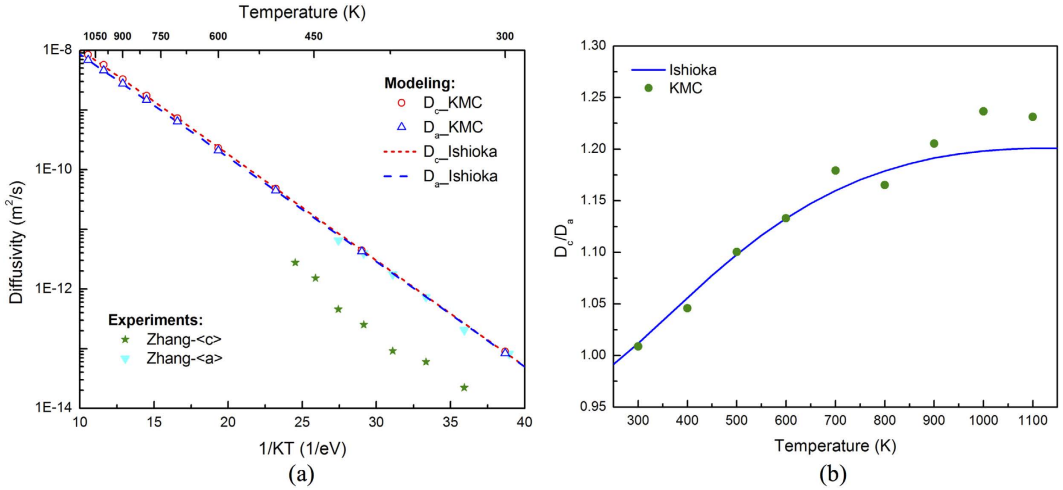

Figure 6. (**a**) H diffusivities along <c> and <a> as functions of inverse temperature, 1/KT. (**b**) D_c/D_a ratio as obtained from KMC simulations and from the Ishioka model from 300 K to 1100 K.

and Zircaloy[14]. This suggests that the H-solute binding might be overestimated in Christensen *et al.*[18], which is possibly due to the neglect of local magnetic moments of Fe and Cr atoms in DFT calculations.

Theoretically, the trapping of impurities can be estimated using the Oriani model[25,35] when the concentrations of the diffuser and impurities are not very high. Specifically, the diffusivity with impurities D_{im} is given by:

$$D_{im} = \frac{D_L}{1 - \sum_i c_t^i + \sum_i c_t^i \exp(E_t^i/K_B T)} \tag{3}$$

Eq. (3) holds when $c_t^i \ll 1$. D_L is the diffusivity without impurities. The physical meanings of other symbols are the same as in Eq. (20) in the Method Section. As shown in Fig. 5, the results from KMC simulations agree well with the Oriani model, while applying which the impurity-free diffusivity D_L is obtained using the Ishioka model and the binding energies in Table 2 are used. According to Eq. (3), alloying elements that are attractive to H, such as Fe, Cr and Ni, reduce H diffusivity. In contrast, solutes such as Sn that are repulsive to H slightly increase H diffusivity. The results from KMC on the separate effect of each element are also in good agreement with the Oriani model, which adopts the same assumptions as used in the mean-field KMC method.

Hydrogen diffusion anisotropy. Due to the hexagonal symmetry of α-Zr, H diffuses anisotropically along <c> and <a> directions, with the latter representing the isotropic 2D diffusion in the basal plane. Since multiple jumps are involved, the anisotropy is not readily evident by just examining the individual hopping rates. KMC simulations allow for the calculation of diffusivity along both <c> and <a> and thus the anisotropy. Moreover, the relative importance of the jump paths can be evaluated at given temperatures to fully elucidate the controversy as reported in previous experiments: $D_c/D_a > 1$ but not exceeding 2 at temperatures above 600 K in Kearns *et al.*[14], and $D_c/D_a < 0.1$ below 500 K in Zhang *et al.*[15]. Even though these experiments were done in different temperature ranges, the data reported were sufficient to establish contradicting trends over a wide range of temperatures.

In KMC simulations, D_c and D_a can be calculated using Eq. (12) by decomposing the MSD into components along <c> and <a>. The results obtained from KMC simulations follow the Ishioka model well, as shown in Fig. 6(b). Some scatter in the KMC results is observed due to the stochastic nature of the KMC method. The D_c/D_a ratio is found to increase with temperature and saturates to about 1.2 at high temperatures (Fig. 6(b)), again agreeing well with the Ishioka model, where the anisotropy is given by:

$$\frac{D_c}{D_a} = \frac{3c^2}{8a^2}\left(\frac{2\omega_{OO}}{3\omega_{OT}} + \frac{2\omega_{TT}}{2\omega_{TT} + 3\omega_{TO}}\right) \tag{4}$$

The temperature dependence in D_c/D_a comes from the temperature dependent hopping rates. At very low temperatures, $\omega_{OO} \ll \omega_{OT}$ and $\omega_{TO} \ll \omega_{TT}$, so that D_c/D_a approaches $3c^2/8a^2$, which is 1.0 for hcp metals with the ideal c/a ratio and about 0.96 for α-Zr using the lattice constants from our DFT calculations. This means that at very low temperatures, $D_a > D_c$ for H in α-Zr. Upon increasing temperature, OO jumps become more important and the first term in the parentheses of Eq. (4) increases. Since the migration barrier for TT jump is significantly lower than that for TO jump (see Table 1), the second term in the parenthesis of Eq. (4) remains close to 1 and only slightly decreases with increasing temperature. The overall trend is that D_c/D_a continuously increases with temperature. As a result, at high temperatures D_c becomes higher than D_a. The transition between $D_c/D_a < 1$ and $D_c/D_a > 1$ occurs at about 270 K. In the above analysis the anisotropic thermal expansion of α-Zr is ignored since its effect is orders of magnitude lower.

Both KMC and the Ishioka model agree with Kearns *et al.*, which predicted $D_c/D_a > 1$ with a ratio no more than 2.0 at temperatures above 600 K[14]. The KMC results on D_a agree perfectly with those measured by Zhang *et al.*

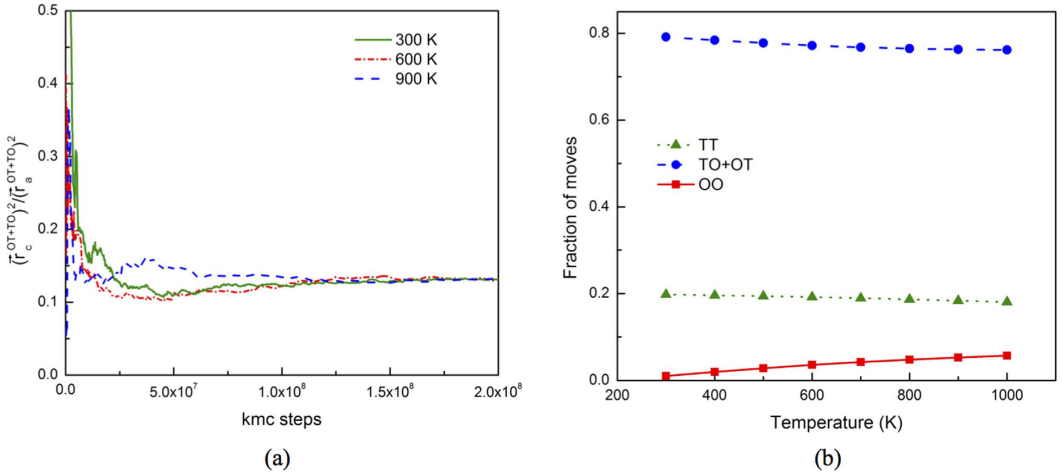

Figure 7. (**a**) Ratio of MSD along <c> over that along <a> induced by TO and OT moves as a function of time at several temperatures. (**b**) Fractions of KMC moves taking TO + OT, TT and OO jumps at various temperatures. Here one TT move represents a basin exit event involving a net TT displacement, not an actual TT move as in regular KMC simulations.

(Fig. 6(a)), where pure single-crystal α-Zr samples were used[15]. However, substantial discrepancy on D_c is noticed. In KMC simulations, D_c is not distinguishable from D_a from 300 K to 500 K, while in the experiments the former was reported to be over an order of magnitude lower than the latter[15] (see Fig. 6(a)). Such a low D_c/D_a ratio is very unlikely if the 3-D, on lattice random walk of H is not altered. H diffusion along <a> is via TO and OT jumps, both with a component along <c> and thus contributing to diffusion along <c>. TT and OO jumps contribute only to <c> diffusion but via two different ways: i) the net displacement induced by these two jumps, and ii) providing a path for H to jump from one <a> plane to another, i.e., bridging TO (OT) jumps in neighboring <a> planes, so that H can perform 3-D random walk. Without the bridging effect, H diffusion will be confined in <a> planes, and the <c> component of TO and OT jumps will cancel each other. During 3-D random walk, the geometry of TO and OT jumps sets a lower bound of D_c/D_a, determined by the ratio of l_c^{OT}/l_a^{OT}; here l_a^{OT} and l_c^{OT} are the components in absolute length of OT jump (or TO) along <a> and <c>, respectively. For H in α-Zr, $l_c^{OT}/l_a^{OT} = l_c^{TO}/l_a^{TO} \approx 0.36$, giving a lower bound of $D_c/D_a = \frac{(l_c^{OT})^2/2t}{(l_a^{OT})^2/4t} \approx 0.26$. Such a geometric effect is independent of temperature except for negligible anisotropic thermal expansion. Indeed, as shown in Fig. 7(a), with sufficient KMC jumps, $(\vec{r}_c^{OT+TO})^2/(\vec{r}_a^{OT+TO})^2$ converges to 0.13 regardless of temperature, corresponding to a D_c/D_a ratio of 0.26. Here, $\vec{r}_c^{OT+TO}$ ($\vec{r}_a^{OT+TO}$) is the total displacement along <c> (<a>) summed over all OT and TO jumps. The KMC analysis also proves our assumption of the 3-D, on-lattice random walk of H, because otherwise $(\vec{r}_c^{OT+TO})^2/(\vec{r}_a^{OT+TO})^2$ cannot converge to 0.13. Note that this ratio is obtained without including the contribution from TT and OO. Therefore, D_c/D_a should be no less than 0.26 as long as H performs 3-D random walk, suggesting that in Zhang *et al.*, D_c was likely be measured at a situation where H diffusion along <c> was suppressed, deviating the random walk behavior. Given the small barrier of TT jump, confined diffusion along <a> is very unlikely in α-Zr or Zircaloy in the dilute concentration regime. Actually, our KMC simulations show that regardless of temperature, TT jumps that bridge two neighboring <a> planes accounts for about 20% of all KMC jumps (Fig. 7(b)), and provides an effective path bridging OT and TO jumps in neighboring <a> planes. Here, each TT jump represents a basin exit event involving a net TT displacement, not an actual TT move as in regular KMC. With increasing temperature, OO jump becomes more important in contributing to <c> diffusion, for its increasing fraction of jumps and long absolute length.

The unreasonably low D_c/D_a ratio measured in Zhang *et al.*[15] may be explained by the so-called blocking layer effect observed in experiments on H in hcp Mg[36]. In Zhang *et al.*, H diffusivity was measured using the surface segregation approach[15]. It is possible that although the matrix H concentration was kept below the solubility limit, the local H concentration near surface could have exceeded that limit when surface segregation occurred. Consequently, precipitation of hydrides such as coherent hydride clusters[37] may have occurred. As the hydrides habit on basal planes with small thickness along <c>, they block H diffusion along <c>, reducing D_c without affecting D_a much, similar to the situation for H in hcp Mg[36].

Discussion

In this section, some discussion is given regarding the comparison between the present results with previous experiments and theories, as well as the applicability of the accelerated KMC method in other material systems.

The diffusivity of H in α-Zr predicted by KMC is at the upper bound of the scatter in the experimental data. The minor discrepancy, which is within the experimental error limit, may come from uncertainties in DFT calculations or in previous experiments. While calculating H vibrational frequencies using DFT, it is assumed that the vibration of H can be decoupled from that of the α-Zr lattice due to the large difference in their masses. Specifically, Zr atoms are fixed in these calculations since their vibration frequencies are orders lower. Minor

error might be induced by such a treatment. For instance, an error of about 0.30 THz (~10 cm^{-1}) was identified for the vibrational frequencies of H (at the order of ~30 THz) on a Ni (111) surface by ignoring lattice atom vibration[38]. Similar anharmonic effect has been noticed for H in α-Zr by Christensen *et al.*[18]. We also note that in the diffusivity calculations (Figs 3 and 5), the effect of quantum tunneling is neglected because its contribution is negligible above room temperature. It should be pointed out that the previous experiments are not exempted from uncertainties either due to the differences in measurement method and sample preparation, as indicated by the scatter in results.

For Zircaloy, again the KMC results are higher but within a factor of 2 than those from experiments. Compared to that in α-Zr, the addition of alloying elements slightly reduces H diffusivity, with negligible effect at high temperatures. This is in line with previous experiments, which found similar H diffusivity in α-Zr, Zircaloy2, and Zircaloy4[14]. The mean-field KMC approach for impurity trapping has two major assumptions. First, Eq. (20) is used assuming that the impurity atom located in the proximity of an H atom modifies only the energy of the initial state without altering the TS. This is inaccurate for H hopping around impurity atoms. However, it still captures the effective migration barrier for an H atom to move away from an impurity atom. To confirm this, the diffusion barrier for an H atom to diffuse away from a Ni atom, from a 1NN tetrahedral site to a 2NN tetrahedral site along <c>, is calculated using DFT. The directly calculated barrier is 0.350 eV, very close to that estimated using Eq. (20), 0.341 eV ($E_b^{T_c}$, 0.212 eV, plus E_m for T-T jump, 0.129 eV). Second, in this work only interaction between H and impurity atoms is considered, with no interactions between H atoms and between impurity atoms. Such an assumption applies when the concentrations of H and impurities are low (i.e., dilute solution). For high H concentration or high impurity concentrations, the interactions between H atoms and between impurity atoms need to be included. The mean-field approximation in Eq. (20) needs to be replaced by more accurate calculations of rate parameters considering local atomic configurations. The same assumptions are shared by the Oriani model[35], which essentially predicts the same results as those from the mean-field KMC.

By comparing KMC with previous theories, this work demonstrates that for hcp metals the Ishioka model is accurate for H diffusivity, and a correction using the Oriani model is sufficient for dilute alloys, provided that all hopping rates are available. However, KMC simulations will be more useful in cases involving spatial heterogeneities, e.g., stress fields induced by cracks and hydrides. The presence of stress fields alters the local solubility and hopping rates as well at each atomic site, making the mean-field approach not applicable.

While the current work focuses on α-Zr and Zircaloy, the same method can be directly applied for H diffusion in other hcp metals such as Mg and Ti and their alloys, where similar diffusion mechanisms and energy basin hold. In Mg, the barrier for T-T jump is about 0.1 eV, much lower than that for T-O (~0.23 eV) and O-O (~0.21 eV) jumps[23]. In Ti, the barrier of T-T jump (0.061 eV) is nearly an order lower than that of T-O (0.424 eV) and O-O (0.625 eV) jumps[2]. H diffusion is critical for H storage in Mg and its alloys[1], and for hydride embrittlement in Ti-based alloys[2]. In a more general sense, the acceleration method applies to interstitial diffusion in hcp metals, or to problems with similar energy basins[39] as shown in Fig. 1(b).

Conclusion

In this work, an accelerated KMC method is developed for efficient calculations of H diffusivity in hcp metals, and demonstrated using H diffusion in α-Zr. Using the hopping rates predicted by DFT, the method accurately predicts H diffusivity in α-Zr and Zircaloy, providing reliable data that could be used for upper scale modeling[5,6]. The results from KMC agree very nicely with previous independent experiments at various temperature ranges[10–15] and the Ishioka theory[22]. The perfect agreement between KMC and Ishioka theory validates the correctness of the analytical equations in this theory. The microscopic diffusion mechanisms obtained from DFT and KMC provide a systematic understanding of H diffusion in α-Zr, which helps to resolve the controversy in previous experiments regarding H diffusion anisotropy. Above room temperature, H diffuses by thermal hopping involving 1NN OT, TT, TO and OO jumps. At low temperatures, an effective diffusion path is via OT- > TT- > TO moves, with the contribution of OO increasing with increasing temperature. The diffusion of H is anisotropic, with the D_c/D_a ratio increasing from below 1.0 at very low temperatures to about 1.20 at high temperatures. In addition to H diffusion in hcp metals, the accelerated KMC method may be applied in other material systems with similar energy basins.

Methods

Residence time lattice kinetic Monte Carlo. In this work we use lattice KMC to calculate the diffusivity of H in Zr. Due to its small atomic size, H stays in Zr as an interstitial, residing in either a tetrahedral or an octahedral site, as shown in Fig. 1(a). A H atom at a tetrahedral site, T_1 for instance, can jump to the neighboring T_2 site (TT jump) or one of the three neighboring O sites (TO). A H atom at an octahedral site, say O_2, can jump to one of the two neighboring O sites (OO), or one of the six neighboring T sites (OT). All these jumps are involved in three-dimensional diffusion. According to the quantum corrected harmonic transition state theory[40], the hopping rate from site *i* to *j* is given by:

$$\omega_{ij} = \frac{K_B T}{h} \frac{Z_{TS}}{Z_i} e^{-E_m/K_B T} \tag{5}$$

Here T is temperature; and h is the Planck constant. E_m is the classical migration barrier associated with the $i- > j$ path. Z_{TS} and Z_i are the partition functions for the transition state (TS) and the initial state. Their ratio accounts for the zero-point energy correction and it is given by:

$$\frac{K_B T}{h} \frac{Z_{TS}}{Z_i} = \frac{\prod_{j=1}^{3} \nu_{i,j} f(h\nu_{i,j}/2K_B T)}{\prod_{k=1}^{2} \nu_{TS,k} f(h\nu_{TS,k}/2K_B T)} \tag{6}$$

where $f(x) = \sinh(x)/x$. Note that Eq. (6) takes into account the ZPE correction at low temperatures and also reproduces the classical hopping rate at high temperatures.

In Eq. (6) $\nu_{i,j}$ ($\nu_{TS,k}$) is the j^{th} (k^{th}) vibrational frequency of H at site i (TS). For each jump, the migration barriers and vibrating frequencies are calculated using DFT calculations at 0 K. The results are listed in Table 1. At each KMC step, the hopping rates are calculated using Eq. (5) for all possible moves. A random number is drawn to pick one jump from the list. The time is advanced following the residence time algorithm by:

$$\Delta t = 1/\sum_j \omega_{ij},\ or\ -\ln(R)/\sum_j \omega_{ij} \tag{7}$$

with R being another random number between 0 and 1. The use of a random number in Eq. (7) better mimics the stochastic nature of kinetic events. With sufficient sampling, the two expressions in Eq. (7) converge to each other.

The above formulation describes diffusion via thermally activated hopping without considering quantum mechanical tunneling, which has been shown to have substantial contribution to H diffusion in some metals at low temperatures[16]. Quantitative prediction of tunneling requires time-consuming calculations of the PES of H interstitial for each jump. Alternatively, assuming that the PES is harmonic at TSs and energy minima, the effect of tunneling can be estimated by applying a semiclassical correction to the hopping rates following the SC-HTST[20,21], given by:

$$\omega_{ij}^{SC} = \omega_{ij}\Gamma_{ij}^{SC} \tag{8}$$

Here ω^{SC}_{ij} is the corrected hopping rate with quantum tunneling, accounted for by the coefficient Γ_{ij}^{SC}. At a given temperature T, Γ_{ij}^{SC} is given by:

$$\Gamma_{ij}^{SC}(T) = \frac{\exp(E_{ZP}/K_BT)}{1+\exp(2\theta_0)} + \frac{1}{2}\int_{-\infty}^{\theta_0} \mathrm{sech}^2\,\theta\,\exp\left(\frac{h\nu_{\pm}\theta}{\pi K_BT}\right)d\theta \tag{9}$$

In Eq. (9), E_{ZP} is the ZPE corrected migration barrier, by

$$E_{ZP} = E_m - \sum_j h\nu_{i,j}/2 + \sum_k h\nu_{TS,k}/2 \tag{10}$$

and $\nu_{\pm}$ is the imaginary vibration frequency at the transition state, given as negative in Table 1. The upper limit of the integration is given by $\theta_0 = \pi E_{ZP}/h\nu_{\pm}$.

To obtain diffusivity, the mean-square-displacement (MSD) of the migrating H atoms at a time t is calculated by:

$$\langle r^2\rangle(t) = \sum_i (r_i(t) - r_i(0))^2/N \tag{11}$$

where N is the number of total H atoms in a KMC simulation, and $r_i(t)$ and $r_i(0)$ are the atomic positions of the i^{th} H atom at time t and time 0, respectively. When multiple H atoms are used in a simulation, they are treated as non-interacting with each other and allowed to overlap, to give the diffusivity in the dilute concentration regime.

Decomposing the total MSD into that along <c> and <a>, the diffusivities along <c>, D_c, and <a>, D_a, can be calculated by:

$$\begin{aligned} D_c &= \langle r_c^2\rangle/2t \\ D_a &= \langle r_a^2\rangle/4t \end{aligned} \tag{12}$$

The different coefficients in the denominator for D_c and D_a are due to the fact that D_a is two-dimensional in <a> plane (normal to <c>), while D_c is one-dimensional along <c>.

The three-dimensional diffusivity is given by:

$$D = \langle r^2\rangle/6t = (\langle r_a^2\rangle + \langle r_c^2\rangle)/6t = (2D_a + D_c)/3 \tag{13}$$

By plotting the MSD as a function of time, diffusivities at various temperatures can be obtained by linearly fitting the MSD curves. Usually, averaging over a large number of independent KMC runs is needed to minimize the stochastic effect.

Acceleration of KMC. For H in hcp metals, the migration barrier of TT jump is usually much smaller than that of TO, OT and OO, forming an energy basin (Fig. 1(b)). At low temperatures, in regular KMC simulations a large fraction of the KMC moves are the back and forth moves between 1NN tetrahedral sites, with zero contribution to the long-range diffusion. This drastically affects the simulation efficiency, assuming that each KMC step costs about the same CPU time. (This assumption holds well for the case here. In general it depends on the number of events at each KMC step and the complexity to calculate the rates of all events). In general, the energy basin problem can be overcome by solving the master equations of the absorbing Markov chain for the occupation probability of the system as a function of time for each transition state[28]. The solutions can be used to replace regular KMC events to improve the efficiency. Following the same method, the expected exiting time and exiting probability for energy basin containing two energy minima (Fig. 1(b)) are derived as:

$$\langle t_{exit} \rangle = \frac{p_2 t_1 + p_2 t_1 p_1 p_3 + p_1 p_4 t_1 + p_1 p_4 t_2}{(1 - p_1 p_3)^2} \tag{14}$$

and

$$\begin{aligned} P_L &= \frac{p_2}{1 - p_1 p_3} \\ P_R &= \frac{p_1 p_4}{1 - p_1 p_3} \end{aligned} \tag{15}$$

Here P_L is the probability for the system to exit to the *left*, i.e., the site from where it enters the basin, and P_R that to the *right*. By definition $P_L + P_R = 1$ once the system exits the basin. t_1 (t_2) are the residence time at the T_1 (T_2) states before next event occurs, which is the time step in a KMC simulation as given in Eq. (7). p_1 (p_3) represents the probability for the system to transition from T_1 to T_2 (T_2 to T_1) in next event. And p_2 (p_4) is the probability for the system to exit the basin from the *left* (*right*) side in next event. By definition $p_1 + p_2 = 1$ and $p_3 + p_4 = 1$.

In pure hcp crystals, the two neighboring T sites (T_1 and T_2 in Fig. 1(b)) are symmetrical and so are the O sites (for each exit in Fig. 1(b) there are three symmetrical O sites) for the H atom to exit to. Therefore, we have $p_1 = p_3$ and $p_2 = p_4$. Similarly, $t_1 = t_2 = t_0$. Eqs (14) and (15) can thus be reduced to:

$$\langle t_{exit} \rangle = \frac{t_0}{p_2} = \frac{1}{\omega_2} \tag{16}$$

and

$$\begin{aligned} P_L &= \frac{\omega_1 + \omega_2}{2\omega_1 + \omega_2} \\ P_R &= \frac{\omega_1}{2\omega_1 + \omega_2} \end{aligned} \tag{17}$$

with ω_i being the hopping rate of the ith jump, as given by Eq. (5). As can be seen from Eq. (17), a H atom always exits with a higher probability from the tetrahedral site where it enters the basin, since $P_L > P_R$ always holds. In cases of $\omega_1 \gg \omega_2$, e.g., at low temperatures, P_R approaches P_L, giving nearly equal probabilities to exit from both T sites. To assure that the diffusion kinetics is preserved during acceleration, it is critical to capture the probability of each exiting path in addition to the basin exiting time. It is also interesting to note from Eq. (16) that for this case the expected exiting time is independent of the barrier between the two minima in the basin.

For acceleration, the KMC events in basins are replaced using the solutions in Eqs (16) and (17). In a KMC simulation with only one H atom, once it enters a basin, it will be taken out in next event, with the exiting path chosen according to Eq. (17). The time advancement is:

$$dt = -\langle t_{exit} \rangle \ln(R) \tag{18}$$

where R is another random number. Statistically, a H atom in a basin will perform $1/p_2$ moves before exiting. Assuming that each KMC step consumes the same CPU time, the acceleration rate of basing exiting time can estimated by the below equation:

$$n_{acc} = \frac{1}{p_2} \tag{19}$$

The above approach is for KMC simulations with one H atom in each. In simulations with multiple H atoms, the same acceleration can be achieved by combining neighboring tetrahedral sites (T_1 and T_2 in Fig. 1(b) for example) into a *super* site (T^*), and modifying the hopping rates towards neighboring octahedral sites based on the path along which a H atom enters the combined T^* site. We note that since the time step is inversely proportional to the number of H atoms used in the simulation, the use of multiple non-interacting H atoms results in no change in the diffusion kinetics and theoretically no change in the efficiency either.

Mean-field impurity trapping. To consider impurity trapping, the mean-field KMC approach[25,26] developed for cubic lattice is extended to hcp, where each impurity atom can trap H in three different ways with different binding energies (see Fig. 1(c)). At each KMC step, the migration barrier of each jump is modified by:

$$E_m = E_m^0 + E_t^i \quad if\ R < c_t^i \tag{20}$$

Here E_m^0 is the barrier without trapping. E_t^i is the binding energy of H at a trapping site t with a concentration c_t^i, induced by impurity i, whose concentration is c_i. R is a random number to be drawn each time when the jump rate is evaluated. The concentration of trapping site t is given by $c_t^i = N_t c_i$, with N_t being the number of trapping sites induced by an impurity atom.

DFT calculations. *Ab initio* calculations are performed using the all-electron projector augmented wave method within the generalized gradient approximation of Perdew, Burke, and Ernzerhof (PBE-GGA)[41], as

implemented in VASP[42]. Large 96-atom supercells, which can be constructed from a $4 \times 4 \times 3$ extension of the 2-atom hcp Zr unit cell, are used throughout our calculations in order to minimize the unphysical interactions between a H atom and its periodic images. A high plane-wave cut-off energy of 500 eV and a dense $5 \times 5 \times 5$ Monkhorst–Pack *k*-point mesh are used to ensure high numerical accuracy for total energy calculations. All internal atomic positions are fully optimized using a conjugate gradient method until forces are less than 0.01 eV/Å. Further relaxations of supercell volumes have been found to have negligible effect on the final results.

Following Domain *et al.*[17], we calculate the H solution energy in Zr as:

$$E_s = E(Zr_N H_1) - E(Zr_N) - \frac{1}{2}E(H_2) \tag{21}$$

Here $E(Zr_N H_1)$ and $E(Zr_N)$ are the total energies of a hcp-Zr simulation cell containing N Zr atoms, with and without a H atom, respectively. $E(H_2)$ is calculated by placing a single hydrogen molecule in a large $10\,\text{Å} \times 10\,\text{Å} \times 10\,\text{Å}$ simulation cell. The equilibrium H-H distance $d_{H\text{-}H}$, vibrational frequency $\nu_{H\text{-}H}$, and dissociation energy $E_{H\text{-}H}$ of of H_2 molecule are calculated to be 0.75 Å, 130.1 THz and 4.54 eV, respectively. These values are in excellent agreement with the experimental values[19] ($d_{H\text{-}H} = 0.74$ Å, $\nu_{H\text{-}H} = 130.8$ THz, and $E_{H\text{-}H} = 4.48$ eV).

The definition used in Eq. (21) is the classical solution energy without considering the ZPE, which should be included when free energy is of interest. The ZPE corrected solution energy can be estimated as:

$$E_s^{ZPE-corrected} = E_s + \sum_{i=1}^{3}\frac{h\nu_i}{2} - \frac{h\nu_{H-H}}{4} \tag{22}$$

The TSs for all diffusion paths of H are obtained using the climbing image nudged elastic band (CI-NEB) technique[43] with 3 intermediate images. Here we only consider 1NN TT, TO, OT and OO jumps since the 2NN jumps are found to be unstable and they spontaneously relax into 1NN jumps. The normal-mode vibrational frequencies of H are obtained from the eigenvalues of the Hessian matrix constructed using finite differences with a small displacement of 0.05 Å. All metal atoms are rigidly constrained during such calculations.

The binding energy between a substitutional solute element X (X = Sn, Fe, Cr, Ni) and an interstitial H atom in hcp Zr can be calculated using the following equation:

$$E_{bind} = E(Zr_{N-1}X_1H_1) + E(Zr_N) - E(Zr_{N-1}X_1) - E(Zr_NH_1) \tag{23}$$

where $E(Zr_{N-1}X_1H_1)$ is the total energy of the supercell containing one impurity atom X and one H interstitial in close proximity of each other. $E(Zr_N)$ and $E(Zr_{N-1}X_1)$ are the total energy of the perfect Zr supercell with N *Zr* and the Zr supercell with a substitutional X atom, respectively. $E(Zr_NH_1)$ is the energy of a Zr supercell with one H occupying the same type of interstitial site as that in the supercell used for $E(Zr_{N-1}X_1H_1)$. As shown in Fig. 1(c), there exist three different 1NN interactions between H and an impurity within 1NN distance. All these interactions are considered in our calculations. For binding between H and Fe, Cr and Ni, spin-polarized calculations have been performed. According to our calculations, Fe and Cr develop large local magnetic moments ($>2\,\mu_B$), while Ni is essentially non-magnetic. The final results are summarized in Table 2.

References

1. Sakintuna, B., Lamari-Darkrim, F. & Hirscher, M. Metal hydride materials for solid hydrogen storage: A review. *International Journal of Hydrogen Energy* **32,** 1121–1140 (2007).
2. Lu, Y. & Zhang, P. First-principles study of temperature-dependent diffusion coefficients: Hydrogen, deuterium, and tritium in α-Ti. *Journal of Applied Physics* **113,** 193502 (2013).
3. Allen, T. R., Konings, R. J. M. & Motta, A. T. Corrosion of zirconium alloys. *Compr. Nucl. Mater.* **5,** 49–68 (2012).
4. Puls, M. P. *The Effect of Hydrogen and Hydrides on the Integrity of Zirconium Alloy Component* (Springer, 2012).
5. Motta, A. T. & Chen, L. Q. Hydride formation in zirconium alloys. *JOM* **64,** 1403 (2012).
6. Bair, J., Zaeem, M. A. & Tonks, M. A review on hydride precipitation in zirconium alloys. *J. Nucl. Mater.* **466,** 12–20 (2015).
7. Kubo, T., Kobayashi, Y. & Uchikoshi, H. Determination of fracture strength of δ- zirconium hydrides embedded in zirconium matrix at high temperatures. *J. Nucl. Mater.* **435,** 222 (2013).
8. Daum, R. S., Bates, D. W., Koss, D. A. & Motta, A. T. *Hydrogen Effects on Material Behaviour and Corrosion Deformation Interactions* (eds. Moody, N. Y. *et al.*) 249–259 (Minerals, Metals and Materials Society, 2003).
9. Dutton, R. S. & Puls, M. P. *Effect of hydrogen on behavior of materials* (TMS-AIME, New York, 1976).
10. Sawatzky, A. The diffusion and solubility of hydrogen in the alpha-phase of zircaloy-2. *J. Nucl. Mater.* **2,** 62 (1960).
11. Schwartz, C. M. & Mallett, M. W. Observations on the behavior of hydrogen in zirconium. *ASM Trans.* **46,** 640 (1954).
12. Mallett, M. W. & Albrecht, W. M. Low-pressure solubility and diffusion of hydrogen in zirconium. *J. Electra-chem. Soc.* **104,** 142 (1957).
13. Someno, M. Determination of the solubility and diffusion coefficient of hydrogen in zirconium. *Nihon Kinzoku Gakkaishi* **24,** 249 (1960).
14. Kearns, J. J. Diffusion coefficient of hydrogen in α-Zr, Zircaloy2 and Zircaloy4. *J. Nucl. Mater.* **43,** 330–338 (1972).
15. Zhang, C. S., Li, B. & Norton, P. R. The study of hydrogen segregation on Zr (0001) and Zr (10-10) surfaces by static secondary ion mass spectroscopy, work function, Auger electron spectroscopy and nuclear reaction analysis. *J. Alloys and Compounds* **231,** 354–363 (1995).
16. Sholl, D. S. Using density functional theory to study hydrogen diffusion in metals: A brief overview. *Journal of Alloys and Compounds* **446–447,** 462–468 (2007).
17. Domain, C., Besson, R. & Legris, A. Atomic-scale ab-initio study of the Zr-H system: I. bulk properties. *Acta Mater.* **50,** 3513 (2002).
18. Christensen, M., Wolf, W., Freeman, C. M., Wimmer, E., Adamson, R. B., Hallstadius, L., Cantonwine, P. E. & Mader, E. H in α-Zr and in zirconium hydrides: solubility, effect on dimensional changes, and the role of defects. *J. Phys. Condens. Matter* **27,** 025402 (2015).
19. Fukai Y. *The metal–hydrogen system* (Berlin: Springer, 1993).
20. Fermann, J. T. & Auerbach, S. Modeling proton mobility in acidic zeolite clusters: II. Room temperature tunneling effects from semiclassical rate theory. *J. Chem. Phys.* **112,** 6787 (2000).

21. Bhatia, B. & Sholl, D. Quantitative assessment of hydrogen diffusion by activated hopping and quantum tunneling in ordered intermetallics. *Phys. Rev. B* **72,** 224302 (2005).
22. Ishioka, S. & Koiwa, M. Diffusion coefficient in crystals with multiple jump frequencies. *Philosophical Magazine A* **52,** 267–277 (1985).
23. Klyukin, K., Shelyapina, M. G. & Fruchart, D. DFT calculations of hydrogen diffusion and phase transformations in magnesium. *Journal of Alloys and Compounds* **644,** 371–377 (2015).
24. Voter, A. F. *Radiation Effects in Solids* (eds. Sickafus, K. E. *et al.*) Ch. 1, 1–23 (NATO Publishing Unit, Dordrecht, Netherlands, 2007).
25. Kirchheim, R. Monte-Carlo simulations of interstitial diffusion and trapping-I: one type of traps and dislocations. *Acta Metall.* **35,** 271–280 (1987).
26. Salomons, E. Monte-Carlo simulation of hydrogen diffusion in metals and alloys. *J. Phys. C: Solid State Phys.* **21,** 5953–5965 (1988).
27. Adelfang, P. & Inozemtsev, V. *Delayed hydride cracking of zirconium alloy fuel cladding, IAEA-TECDOC-1649* (International Atomic Energy Agency, Vienna, 2010).
28. Puchala, B., Falk, M. L. & Garikipati, K. An energy basin finding algorithm for kinetic Monte Carlo acceleration. *The Journal of Chemical Physics* **132,** 134104 (2010).
29. Burr, P. A., Murphy, S. T., Lumley, S. C., Wenman, M. R. & Grimes, R. W. Hydrogen accommodation in Zr second phase particles: implications for H pick-up and hydriding of zircaloy2 and zircaloy4. *Corros. Sci.* **69,** 1–4 (2013).
30. Udagawa, Y., Yamaguchi, M., Abe, H., Sekimura, N. & Fuketa, T. Ab initio study on plane defects in zirconium-hydrogen solid solution and zirconium hydride. *Acta Mater.* **58,** 3927 (2010).
31. Goldak, J., Lloyd, L. T. & Barrett, C. S. Lattice parameters thermal expansions and gruneisen coefficients of zirconium 4.2 to 1130 degrees K. *Phys. Rev.* **144,** 478 (1966).
32. Zuzek, E., Abriata, J., San-Martin, A. & Manchester, F. The H-Zr (hydrogen-zirconium) system. *Bull. Alloy Phase Diagr.* **11,** 385 (1990).
33. Lumley, S. C., Grimes, R. W., Murphy, S. T., Burr, P. A., Chroneos, A., Chard-Tuckey, P. R. & Wenman, M. R. The thermodynamics of hydride precipitation: the importance of entropy, enthalpy and disorder. *Acta Mater.* **79,** 351 (2014).
34. Kearns, J. J. Terminal solubility and partitioning of hydrogen in the alpha phase of zirconium, zircaloy-2 and zircaloy-4. *J. Nucl. Mater.* **22,** 292–303 (1967).
35. Oriani, R. The diffusion and trapping of hydrogen in steel. *Acta Metall.* **18,** 147–157 (1970).
36. Uchida, H. T., Kirchheim, R. & Pundt, A. Influence of hydrogen loading conditions on the blocking effect of nanocrystalline Mg films. *Scripta Materialia* **64,** 935–937 (2011).
37. Zhang, Y. F., Bai, X. M., Yu, J., Tonks, M. R., Noordhoek, M. J. & Phillpot, S. R. Homogeneous hydride formation path in α-Zr: Molecular dynamics simulations with the charge-optimized many-body potential. *Acta Materialia* **111,** 357–365 (2016).
38. Greeley, J. & Mavrikakis, M. A first-principles study of surface and subsurface H on and in Ni(111): diffusional properties and coverage-dependent behavior. *Surface Science* **540,** 215–229 (2003).
39. Xu, L. J. & Henkelman, G. Adaptive kinetic Monte Carlo for first-principles accelerated dynamics. *J. Chem. Phys.* **129,** 114104 (2008).
40. Katz, L., Guinan, M. & Borg, R. J. Diffusion of H2, D2, and T2 in single-crystal Ni and Cu. *Phys. Rev. B* **4,** 330 (1971).
41. Perdew, J. P., Burke, K. & Ernzerhof, M. Generalized gradient approximation made simple. *Phys. Rev. Lett.* **77,** 3865 (1996).
42. Kresse, G. & Furthmuller, J. Efficient iterative schemes for ab initio total-energy calculations using a plane-wave basis set. *Phys. Rev. B* **54,** 11169 (1996).
43. Henkelman, G., Uberuaga, B. P. & Jonsson, H. A climbing image nudged elastic band method for finding saddle points and minimum energy paths. *J. Chem. Phys.* **113,** 9901 (2000).

Acknowledgements

The INL authors gratefully acknowledge the support of the INL Laboratory Directed Research and Development Program under project #14-026, "Multiscale modeling on delayed hydride cracking in zirconium: hydrogen transport and hydride nucleation", and the Department of Energy (DOE) Nuclear Energy Advanced Modeling and Simulation (NEAMS) program. This manuscript has been authored by Battelle Energy Alliance, LLC under Contract No. DE-AC07-05ID14517 with the U.S. Department of Energy. The United States Government retains and the publisher, by accepting the article for publication, acknowledges that the United States Government retains a nonexclusive, paid-up, irrevocable, world-wide license to publish or reproduce the published form of this manuscript, or allow others to do so, for United States Government purposes. All authors are grateful to Dr. Larry Aagesen at INL who provided proofreading and valuable comments.

Author Contributions

Y.Z., C.J. and X.B. initiated the research idea together. C.J. conducted the DFT calculations. Y.Z. and C.J. performed KMC simulations. Y.Z. wrote the manuscript with the help of C.J. and X.B. All authors contributed to data analysis and discussions.

Additional Information

Competing financial interests: The authors declare no competing financial interests.

How to cite this article: Zhang, Y. *et al.* Anisotropic hydrogen diffusion in α-Zr and Zircaloy predicted by accelerated kinetic Monte Carlo simulations. *Sci. Rep.* **7**, 41033; doi: 10.1038/srep41033 (2017).

Publisher's note: Springer Nature remains neutral with regard to jurisdictional claims in published maps and institutional affiliations.